Manufacturability-Driven Multi-Component Topology Optimization Of Thin-Walled Structures Based On A Level Set Method

by

Samuel Ayinde

A dissertation submitted in partial fulfillment
of the requirements for the degree of
Doctor of Philosophy
(Mechanical Engineering)
in The University of Michigan
2020

Doctoral Committee:

Professor Kazuhiro Saitou, Chair
Assistant Professor Jesse Austin-Breneman
Assistant Professor Daniel Cooper
Assistant Professor Evgueni Filipov

Samuel Ayinde

sayinde@umich.edu

ORCID iD: 0000-0001-6569-2755

DEDICATION

To the Father, Son and the Holy Spirit.

For seeing me through this journey

For been my Guide at every turning

When the path was smooth and when it was thorny

To You belong all the glory

ACKNOWLEDGEMENTS

I would like to express my profound gratitude to my advisor, Professor Kazuhiro Saitou for his tremendous contributions to the success of my PhD program. Time and again, he went the extra mile to ensure that I am able to solve the problems and overcome the obstacles I encountered all through the journey. I also want to appreciate my committee members, Professor Jesse Austin-Breneman, Professor Daniel Cooper and Professor Evgueni Filipov for their unique contributions to the success of my PhD program. Their special contributions helped in improving the quality of my research and the dissertation. I appreciate them for taking time out of their engaged schedules to give me timely and crucial inputs. Special thanks to Professor Chinedum Okwudire, Professor Elijah Kannatey-Asibu and Professor Lola Eniola-Adefeso for their mentoring and counseling on how to navigate the winding road of graduate school. I want to appreciate Dr Yuqing Zhou, Professor Bing Yi, Professor Gil Ho Yoon and Dr Gregory Teichert for their insightful contributions and their efforts while on the journey. My research has received financial support from National University Commission (NUC) under Presidential Special Scholarship Scheme for Innovation and Development (PRESSID) and Petroleum Technology Development Fund (PTDF) in Nigeria; and The University of Michigan, Ann Arbor. These sources of support are thankfully acknowledged. I will like to appreciate my family, friends and loved ones for their support, encouragement and prayers. Above all, I return all thanks, praises, glory, honor and adoration to the Almighty God, Who was, Who is and Who is to come. Thank you Lord for been my All-In-All.

TABLE OF CONTENTS

LIST OF FIGURES

LIST OF TABLES

LIST OF APPENDICES

ABSTRACT

Thin-walled structures (TWS) are suitable for lightweight, load-bearing enclosures with various external geometries with internal reinforcements. Thin-walled structures find application in automobiles, aircrafts, ships, and industrial facilities. Past research in the field of structural design optimization have been done to make single-piece thin-walled structures less costly, lighter and of better performance. The primary drawback of these research is that complex structures are scarcely manufactured as a single piece, and this has made the optimization of single-piece structures to be of little industrial relevance.

The goal of this dissertation is to develop a computational method for simultaneous design and partitioning of assemblies made of thin-walled components, driven by component manufacturability. First, the conventional level set function for monolithic topology optimization based on a signed distance function is extended to realize a simple representation of monolithic thin-walled structures with uniform thickness, by taking advantage of the signed-distance property. Second, a new multi-domain representation within a level set, inspired by level-set methods for multi-material topology optimization, is introduced to model multiple components, where the additional level sets specify partitioning of the level set for a monolithic thin walled structures. Finally, the geometric constraints imposed by a manufacturing process for thin-walled components, sheet metal stamping as an example, are introduced to formulate the manufacturability-driven, multi-component topology optimization of thin-walled structures. The

optimization problem is formulated as continuous optimization with respect of the level set parameters that specify overall structural geometry and its partitioning, which can be solved efficiently by gradient-based optimization algorithms. A few examples inspired by the sheet metal structures for automotive applications demonstrated the effectiveness of the new formulation to automatically design thin-walled structures made of multiple component each of which satisfies process-specific geometric constraint for component manufacturing. The conventional approach for design and partitioning is a two-step process in which the optimization of the single-piece geometry is first carried out, followed by the decomposition of the optimized single-piece geometry to refine part boundaries and joint configurations. Since the outcome of the second step largely depend on the first step, the two-step approach is likely to yield suboptimal solution. Although the improvement resulting from the new formulation of simultaneous design and partitioning cannot be quantify, it is expected to bring about improvement when joint modeling is implemented.

This dissertation advances the state of the art of the simultaneous designing and partitioning of thin-walled structures driven by manufacturability. While the dissertation focuses on the auto-body application, it is expected that the methodology will be applicable to other domains of thin-walled structures.

CHAPTER 1

Introduction

Thin-walled structures are suitable for lightweight, load-bearing enclosures with various external geometries with internal reinforcements. These include cars, trains, planes, ships, oil rigs, storage vessels, industrial buildings and warehouses. Some examples are shown in Figure 1.1.

(a)

(b)

(c)

(d)

Figure 1. 1 Examples of thin-walled structures. (a) Car [1], (b) Building [2], (c) Storage vessel [3], and (d) Aircraft [4]

Thin-walled structures are typically made of stamped and trimmed rolled metal sheets with a constant thickness joined by welding and/or riveting, as illustrated in Figure 1.2. Conventional sheet metal stamping process involves the use of dedicated dies to shear pieces of required external shapes (i.e., blanks) from metal stock, followed by using the dies to change the shape of the blanks by stretching, compressing, bending and to include additional features through piercing operations.

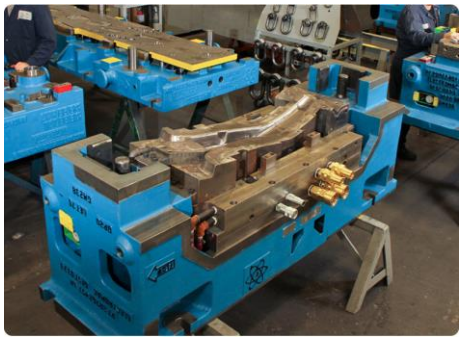

(a)

(b)

Figure 1. 2 Typical manufacturing processes for thin walled structures. (a) Stamping of a car body [5], and (b) Welding operation on a car body [6]

Due to its importance in many product segments, numerous research has been carried out to make thin-walled structures lighter, better and less expensive ([7]–[11]). Taking automobile as an example, heavier vehicles consumes more fuel. A 10% weight reduction results in about 7% fuel economy [12]. Also, heavier vehicles increase the risk of other vehicles into which they crash. Further, increasing societal pressure for CO_2 reduction demands lighter structures with improved performance at a lower cost.

Topology optimization [13] provides a viable approach to reduce the overall weight of thin-walled structures while simultaneously obtain a better performance. Topology optimization tries to answer this question: given a prescribed design domain, how can the materials be optimally

distributed to obtain a better structural performance under certain constraints? This non-parametric geometric representations peculiar to topology optimization gives it an advantage over the parametric representations of size and shape optimization, since the optimization can explore truly arbitrary geometry within the domain.

Multi-component structural product is conventionally designed using two-step approach. First, the overall single-piece geometry is designed and optimized. Second, the optimized single-piece design is decomposed to refine part boundaries and joint configurations. However, since the second step is largely dependent on the result of the first step, the two-step approach is likely to result in suboptimal results as regards the overall structural performance or manufacturing cost or both.

The goal of this dissertation is to advance the computational optimal design method for thin-walled structural assemblies with emphasis on the manufacturability of each component. This research enables simultaneous designing and partitioning of thin-walled structural assemblies. Unlike the two-step approach, this formulation is simultaneously designing the geometry and partitioning it into multiple components. This new formulation is expected to perform better with the implementation of joint modeling. This research focuses on the auto-body application, that is, stamped sheet metal components joined by resistance spot welding. The methodology however is expected to be applicable to other domains of thin-walled structures.

This dissertation is arranged as follows. Section 1 is on the introduction of thin-walled structures. Section 2 gives a review of previous works related to this research. In Section 3, the goal of the dissertation is discussed. Section 4 discusses the approach. The numerical examples are presented in Section 5. Section 6 is on Joint model. The conclusion of the dissertation is presented in Section 7.

CHAPTER 2

Literature Review

2.1 Topology Optimization

Structural topology optimization (TO) tries to answer this question: Given a design domain and certain constraints, how can material(s) be distributed within the prescribed design domain to achieve a particular structural performance or satisfy certain requirement [14]? This material distribution approach to topology optimization was proposed by Kikuchi and Bendsøe [13]. Non-parametric geometric description peculiar to topology optimization makes it possible to explore arbitrary design shapes and obtain novel designs (Figure 2.1).

Figure 2. 1 Examples of Topology Optimization results. (Sources: Left to right. [15], [16], [17])

This gives it an advantage over sizing and shape optimization that are usually based on parametric geometric descriptions [18]. There are several methods for formulating and solving topology optimization problems. These include Homogenization method ([13], [19]–[21]), Solid Isotropic Material with Penalization (SIMP) method ([18], [22]–[24], [22], [25]), level-set method ([26]–[30]) based on topological derivatives ([31]–[34]) or shape derivatives ([35]–[38]) [39], moving morphable components method ([40]–[43]) [42], evolutionary structural

optimization (ESO) method ([44]–[47]) , bidirectional evolutionary structural optimization (BESO) method ([48]–[51]) , and topology optimization using non-gradient optimization algorithms ([52]–[55]) [56].

Figure 2. 2 (a) Discrete topology optimization [57] (b) Continuous topology optimization [58]

Topology optimization can be solved in the discrete design domain [59] (Figure 2.2 (a)) or continuum design domain [60] (Figure 2.2 (b)). Certain products with complex geometries are easy to represent in the continuum design domain, and for such cases, this gives it a leverage over discrete design approach. Application of non-gradient method in the continuum design domain has been criticized because the computational cost could be very high in high resolution designs ([52], [60], [61]. Beside structural design problems, topology optimization also find application in other areas such as fluid mechanics [62] and microsystems [63].

2.2 Manufacturability-driven topology optimization

A major challenge encountered in the earlier work on topology optimization is in the area of the manufacturability of the optimized design. This challenge limited the application of topology optimization results primarily to acquiring academic knowledge with little industrial relevance. An earlier example of such non-manufacturable results for topology optimization is the ones with checkerboards patterns (Figure 2.3) emanating from numerous small holes below the tolerance of available manufacturing processes [64].

Figure 2. 3 Checkerboard pattern [64]

Problems related to the checkerboards pattern have been solved using regularization schemes such as constraint methods [65] and filtering methods ([66], [67]), thereby resulting in simpler geometries, improved numerical stabilities and better manufacturability in a general sense.

To make an optimized design conform to a particular manufacturing process, process-specific geometric constraints are incorporated into the optimization formulation, which ensures convergence to the final design that is manufacturable by the manufacturing process. For instance, constant cross-section along a direction is necessary and is formulated as a constraint for optimizing a product manufactured by extrusion [68]. For molding and casting, the necessary constraint is that the design must be free from fully-enclosed cavities and undercut in the die's draw direction ([23], [69]). The authors in [70] proposed a method to optimize structures with discrete geometric primitives with the aim of facilitating the manufacturing processes tailored to plate structures. For additive manufacturing, different overhanging constraints were developed to reduce the amount of supports required during the printing process [71].

2.3 Design optimization of stamped sheet metal components

For sheet metal components to be economically manufacturable, the design must be well thought-out. Up to 50% of the manufacturers' time is spent on fixing errors and 24% of those errors are related to manufacturability [72]. These errors result from the gap between the sheet-metal parts designing procedures in the CAD systems and the actual manufacturing on the shop floor. In order

to close this gap, design for manufacturability (DFM) guidelines for sheet metal designs have been developed ([73]–[75]) which enabled the designers to consider important manufacturability factors while developing sheet metal designs. In [76], the structural stiffness parameter of sheet metal are optimized and the forming quality of the optimized design is examined for the stamping process using commercial software. The author in [77] studied the impact of sheet metal stamping on the crashworthiness of sheet metal part and optimized the stamping properties and crashworthiness using a genetic algorithm.

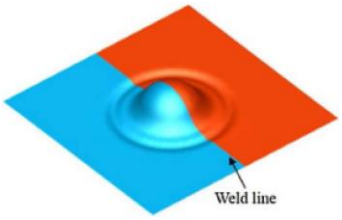

Figure 2. 4 Example of TWB [78]

Some work addressed the optimization of sheet metal components stamped from tailor-welded blank (TWB), a metal sheet made of multiple sheets with different thicknesses that are weld together prior to stamping [79]. In [80], bidirectional evolutionary structural optimization (BESO) method was used for the optimal design of an automotive door with multiple thicknesses for the optimal thickness layout and welding line locations. Song and Park [81] used multidisciplinary design optimization to reduce the weight of an automotive door made of TWB subject to a stiffness constraint, and side impact and natural frequency constraints. Using Taguchi-based gray relational analysis, Xu *et al*. [82] proposed a discrete optimization of tailor-welded blanks (TWBs) structures with top-hat thin-walled section subjected to front dynamic impact. Jie *et al.* [83] focused on optimal stiffener layout design of thin-walled structures subject to multi-fastener joint loads and manufacturing constraints. The difference of the material properties in the thermal influence zone

(weld) of TWB poses challenges such as stress concentration, possibility of fatigue failure and a significant wearing of the tool by the seam ([84], [85]). Tailor-rolled blank (TRB) (Figure 2.5) is developed to overcome these challenges, thereby ensuring a continuous transitioning between different material properties zones and a higher surface quality [79].

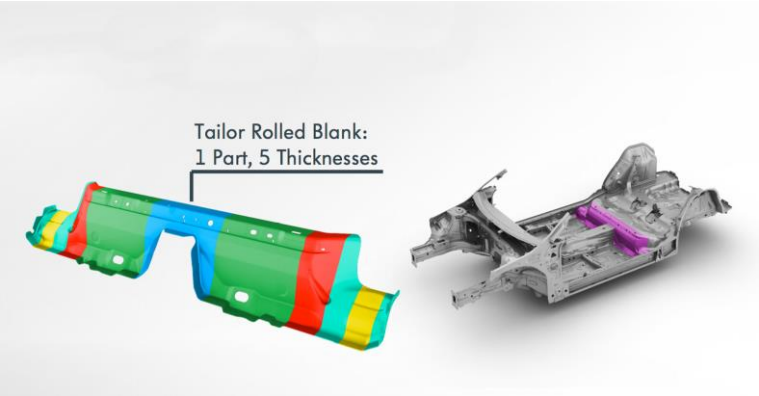

Figure 2. 5 Tailored rolled blank [86]

In an effort to design sheet metal components for improved performance without increasing the material cost, beads are often introduced on their surfaces ([87]–[89]). See Figure 2.6. Beads increase the stiffness of the sheet metal in bending. Attempts to determine the optimal geometry, position, and orientation of beads give rise to *topography optimization*. Topography optimization optimizes the topography of a surface in 3D space by allowing the modification of the sub regions of the surface in a specified direction, and can represent the realistic "2.5D" geometry (flattenable with small distortion) of thin-walled components manufactured by the stamping process. Alshabatat *et al.* [90] used spherical dimples and cylindrical beads to alter the local stiffness of plates while keeping the overall plate mass constant. Using the combination of the finite element method and an optimization procedure based on the genetic algorithm, the optimal design of beads and dimples for the improvement of the natural frequencies of the plates can be determined.

SIMULI *Tosca*, ALTAIR *Solidthinking*, and VR&D *Genesis* are the examples of commercial software for implementing topography optimization or bead insertions, as shown in Figure 2-6.

(a) (b)

Figure 2. 6 Topography Optimization using (a) Solidthinking [91], and (b) Tosca [92]

The major drawback of these works, however, is that they are limited to monolithic thin-walled structures, and cannot handle simultaneous designing and partitioning of thin-walled assemblies.

2.4 Design optimization of monolithic coated structures

The essence of coating treatment is to protect the substrate structure from adverse work environment such as very high temperature, corrosive environment or extreme weather conditions. A few recent papers addressed the optimal design of monolithic thin-walled structures represented as coating on the surface of bulk solid geometry. Clausen *et al*. [93] achieved the minimum compliance topology optimization of coated structures by using solid isotropic material with penalization (SIMP) method ([22], [25]). They proposed the use of series of filter, projection, and gradient normalization for modeling the coating layer with a near-uniform thickness on the substrate surface. Wang and Kang [39] leveraged the signed distance property of level set to implement the topology optimization of a coated structure, with a single level set defining the coating domain, substrate domain, void domain and the interfaces between them. An example of the results from their approach is shown in Figure 2.7. Similar to coating, Dienemann *et al*. [94]

adopted a mid-surface representation for optimizing thin-walled structural topology with cut-outs, which can be manufactured by a single-step deep drawing. They later added manufacturing constraints for minimum corner radius and a maximum tearing risk to the topology optimization of deep drawable sheet metals [95]. An example of their optimized result is shown in Figure 2.8.

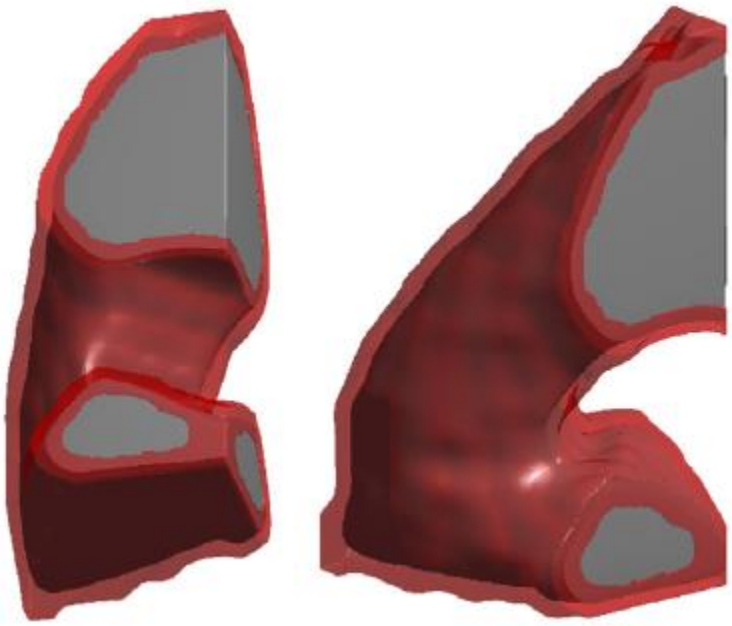

Figure 2. 7 Sections of a 3D coated structure [39]

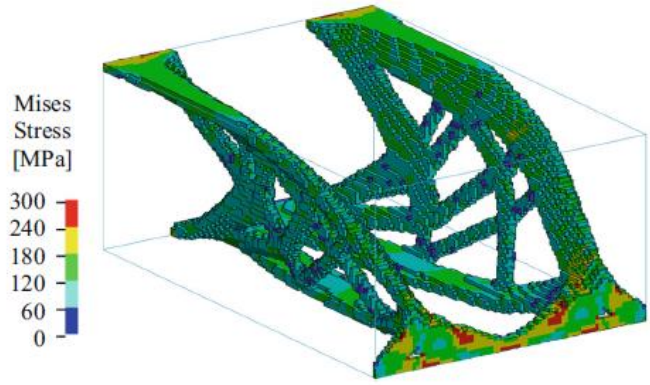

Figure 2. 8 Optimized cantilever beam with manufacturing constraint [23]

Similar to the works listed in the previous section, these works are limited to monolithic thin-walled structures, and cannot handle simultaneous designing and partitioning of thin-walled assemblies.

2.5 Design optimization of sheet metal assemblies

The design of sheet metal assembly has been traditionally carried out following the requirement flow-down approach in systems engineering [96], which relies on the manual inputs for component boundaries. In the past decades, however, attempts have been made to apply computational optimization for the top-down design of sheet metal assemblies as a whole. Yetis and Saitou [55] presented a two-step approach for the optimization of the topology of an entire structure and the location and configuration of joints, considering strength, manufacturability, and assembleability. Lyu and Saitou [54] presented the optimal partitioning of automotive body-in-white (BIW) model into a set of components considering the stiffness of the assembled structure, as well as the manufacturability and assembleability of components, as illustrated in Figure 2.9.

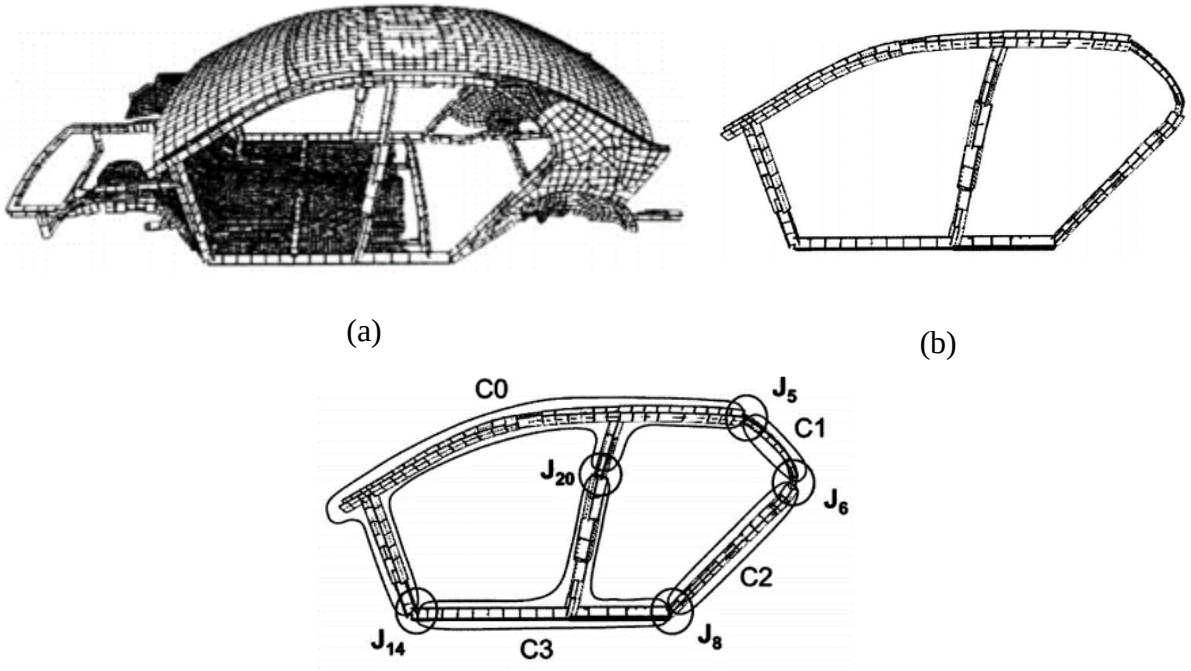

Figure 2. 9 (a) BIW, (b) Side frame of the BIW, and (c) Four-component decomposition [53]

These works, however, are limited to the analysis of an assembly with a given geometry and partitioning, or the optimal partitioning of a given geometry based on manufacturability of components, and do not implement simultaneous design and partitioning.

2.6 Simultaneous optimization of design and partitioning

Simultaneous optimization of topology design and partitioning has been proposed for several classes of structures, including thin-walled structures. Lyu and Saitou [97] proposed a method for simultaneous optimal design of cross sections and joints in the space frame body structures of passenger vehicles. Solved with a multi-objective genetic algorithm, the method can simultaneously determine the locations and types of joints in a structure and the cross sections of the joined structural frames. The manufacturing cost and assembly cost are estimated from the geometry of the components and joints.

Multicomponent topology optimization (MTO) focus on obtaining optimal structures made as assemblies of near-manufacture multiple components, with each component subject to geometric constraints imposed by a chosen manufacturing process ([23], [24], [58]). It can be seen as a close relative of multi-material topology optimization ([98], [29], [30], [99]) which deals with the simultaneous optimization of the base topology of monolithic structure and the distribution of multiple materials within it. However, multi-material topology optimization focuses on optimizing the structural performance without explicit constraints on the distribution of each material domain.

An early attempt of MTO is found in [53], where simultaneous optimization of the topology and partitioning of a planar structure over a discrete ground structure with non-overlapping beams was presented for structural stiffness, total weight, and component manufacturability. Yildiz and Saitou [52] presented a relaxation of this work to a continuum design domain. With the aim of reducing the computational cost, Guirguis *et al*. [60] and Guirguis and Aly [100] used the Kriging-interpolated level-set to represent the base topology and its partitioning, which significantly reduced the number of design variables and improved the computational efficiency. To obtain an improved performance of the Genetic Algorithm used for optimization, Zhou *et al*. [101] proposed a mutation operator based on portioning templates and localized joint morphing. A major drawback of these works however, is the problem formulation as discrete optimization, which makes them to be computationally extremely inefficient.

In an attempt to overcome these limitations, Zhou and Saitou [24] proposed a continuous optimization formulation that integrated partitioning into a conventional gradient-based SIMP framework of topology optimization [22], by introducing new design variables that specify fractional membership to each component. This formulation has also been employed to the

multicomponent topology optimization for additive manufacturing with constraints on build volume and cavity-free components [102]; multicomponent topology and material orientation design of composite structures [58]; multicomponent topology optimization for die casting [23]; and, anisotropic multicomponent topology optimization for additive manufacturing with build orientation design and stress-constrained interfaces [103].

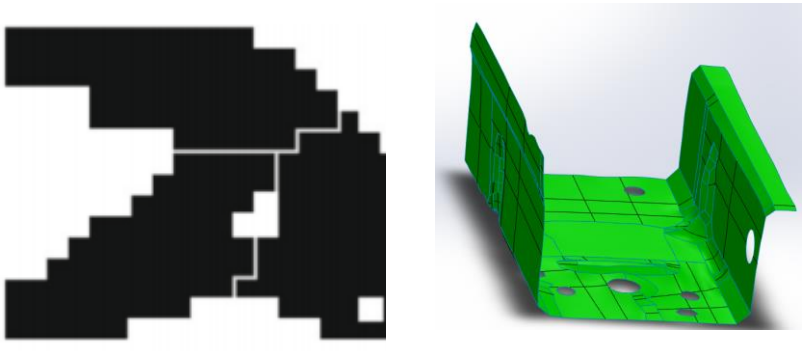

(a) (b)

Figure 2. 10 (a) 2D sheet metal assembly in [24] and (b) typical 2.5D thin-walled structure (Toyota Venza part)

While the compliance minimization of sheet metal assemblies subject to manufacturing constraints is presented in [24], this work is limited to two-dimensional geometries. In particular, its formulation is based on a 2D (*i.e.*, planar) version of 3D solid geometry (Figures 2.10 (a)), and is not compatible to the "2.5D" geometry (Figures 2.10 (b)), which is typical for manufacturing processes for thin-walled components such as sheet metal forming.

CHAPTER 3

Dissertation Goal

The goal of this dissertation is to develop a computational method for simultaneous design and partitioning of assemblies made of thin-walled components driven by component manufacturability.

To this aim, the following Research Questions are addressed:

1. What is the geometric representation suitable for thin-walled structures with arbitrary surface topology and geometry with a constant thickness?
2. What is the geometric representation suitable for multiple subdomains (components) with arbitrary topology and geometry on the thin-walled structures in 1?
3. How can 1 and 2 be integrated with the constraints on the subdomain geometry imposed by component manufacturability, to formulate the simultaneous optimization of design and partitioning of thin-walled structures? Manufacturing constraint on the components is the driver of this formulation.

For Research Question 1, the conventional level set function for monolithic topology optimization based on a signed distance function ([35], [37], [104]–[106]) is extended to realize a simple representation of monolithic thin-walled structures with uniform thickness, by taking advantage of the signed-distance property. Research Question 2, a new multi-domain representation within a level set, inspired by level-set methods for multi-material topology optimization ([29], [107], [108]), is introduced to model multiple components, where the additional level sets specify

partitioning of the level set for a monolithic thin walled structures. Research Question 3, the geometric constraints imposed by a manufacturing process for thin-walled components, sheet metal stamping [24] as an example, are introduced to formulate the manufacturability-driven, multi-component topology optimization of thin-walled structures. The optimization problem is formulated as continuous optimization with respect of the level set parameters that specify overall structural geometry and its partitioning, which can be solved efficiently by gradient-based optimization algorithms.

CHAPTER 4

Approach

4.1 Level set method for topology optimization

Level set method (LSM) [106] is a method commonly used for representing a moving interface of a domain, whose velocity depends on the position, time, interface geometry and external physics [109]. Boundary Γ that bounds a domain Ω is represented as the zero level set of a function, which is positive inside Ω and negative outside Ω. LSM has been used to represent structural topology in topology optimization, where a level set function $\phi: D \rightarrow \boldsymbol{R}$ defines the interfaces between material domain Ω and void domain $D \backslash \Omega$ ([27], [35]) as,

$$\begin{cases} \phi(x) > c \text{ if } x \in \Omega \\ \phi(x) = c \text{ if } x \in \Gamma \\ \phi(x) < c \text{ if } x \in D \backslash \Omega \end{cases} \tag{4-1}$$

where c is a constant, usually zero, and x is a point in a prescribed extended design domain D.

Figures 4.1(a) show an example of level set and the corresponding structural topology of a cantilever beam (Figure 5-3a), where green color represents material and white color represents void in Figure 4.1(b).

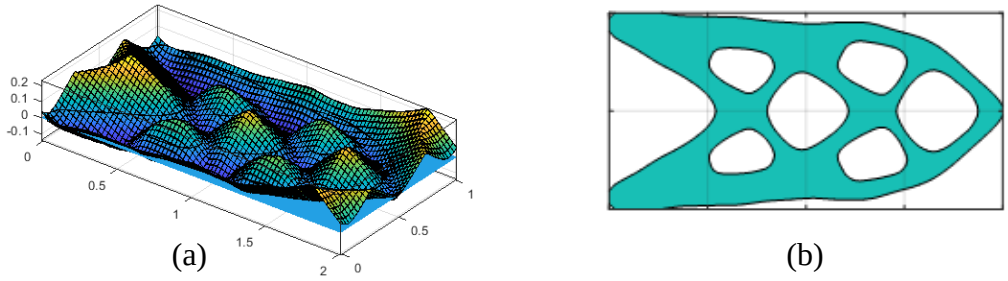

(a) (b)

Figure 4. 1 (a) Example of a level set function in 3D and (b) Its corresponding 2D representation depicting the topology optimization result for the cantilever in Figure 5.3(a)

The most commonly used LSF in topology optimization is implicitly defined as a signed distance function, which is usually updated using Hamilton-Jacobi equations:

$$f(x) = \begin{cases} d(x,\Gamma) \text{ if } x \in \Omega \\ -d(x,\Gamma) \text{ if } x \in D \backslash \Omega \end{cases} \tag{4-2}$$

where d is the distance between point x in D and Γ. Other representations include implicit functions defined by reaction-diffusion equations ([32], [110]), and explicit functions by Kriging interpolation ([61], [111], [112]) and radial basis functions [113]. Optimization methods used include gradient-based methods ([32], [39], [93]) based on shape derivatives ([36], [38], [39]) or topological derivatives ([32], [34]) and non-gradient methods ([48], [101]). In contrast to the density formulation where the boundary of structures is not clearly defined prior to the convergence of optimization, the level set method gives the clear boundary at the onset.

Townsend and Kim [114] applied the level set topology optimization method for the buckling of shell structure. The formulation is equally applicable to the structures with binary thickness distribution, such as two-thickness plates, and structures with cut-out. In [115], the level set method is applied to the structural topology optimization of platelike wings under flutter and divergence constraints. For the application of level set topology optimization method to stress-

related problem, interested readers are referred to ([116]–[119]). In [120], level set method incorporating topological derivatives is applied to the topology design of compliant mechanisms under von Mises stress constraints. Dunning and Kim [121] proposed a sequential linear programming level set topology optimization method to handle multiple constraints and simultaneously optimize non-level-set design variables. This method was applied to solve problems involving volume, compliance, eigenvalue and displacement constraints and simultaneous optimization of non-level-set design variables. For the application of level set method to topology optimization of multimaterial structures, interested readers are referred to ([29]–[31], [99], [107], [108]).

4.2 Representation of monolithic thin-walled structures

In this dissertation, the level set method is adopted as the representation of TWS due to its signed-distance property that can naturally represent structures with constant wall thickness without additional constraints.

It is assumed that most thin-walled structures can be represented as a pair of closed offset surfaces with holes, whose example is shown in Figure 4.2.

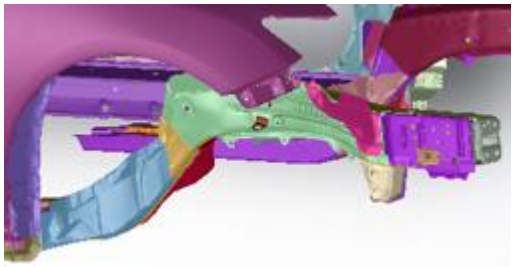

Figure 4. 2 Example of thin-walled subassemblies of Toyota Venza

A signed distance level set function ϕ_1 is used to represent a pair of closed offset surfaces with a prescribed distance t, and another level set ϕ_2 is used to represent holes on the offset surfaces, as

illustrated in Figure 4.3. Thanks to the characteristic of signed-distance function in Eq (4-2), the leveled boundary at $\phi_1 = t$ is guaranteed to be equidistance from the levelled boundary at $\phi_1 = 0$. This eliminates the need of additional constraint for constant wall thickness, which would be otherwise required during the optimization of ϕ_1 and ϕ_2.

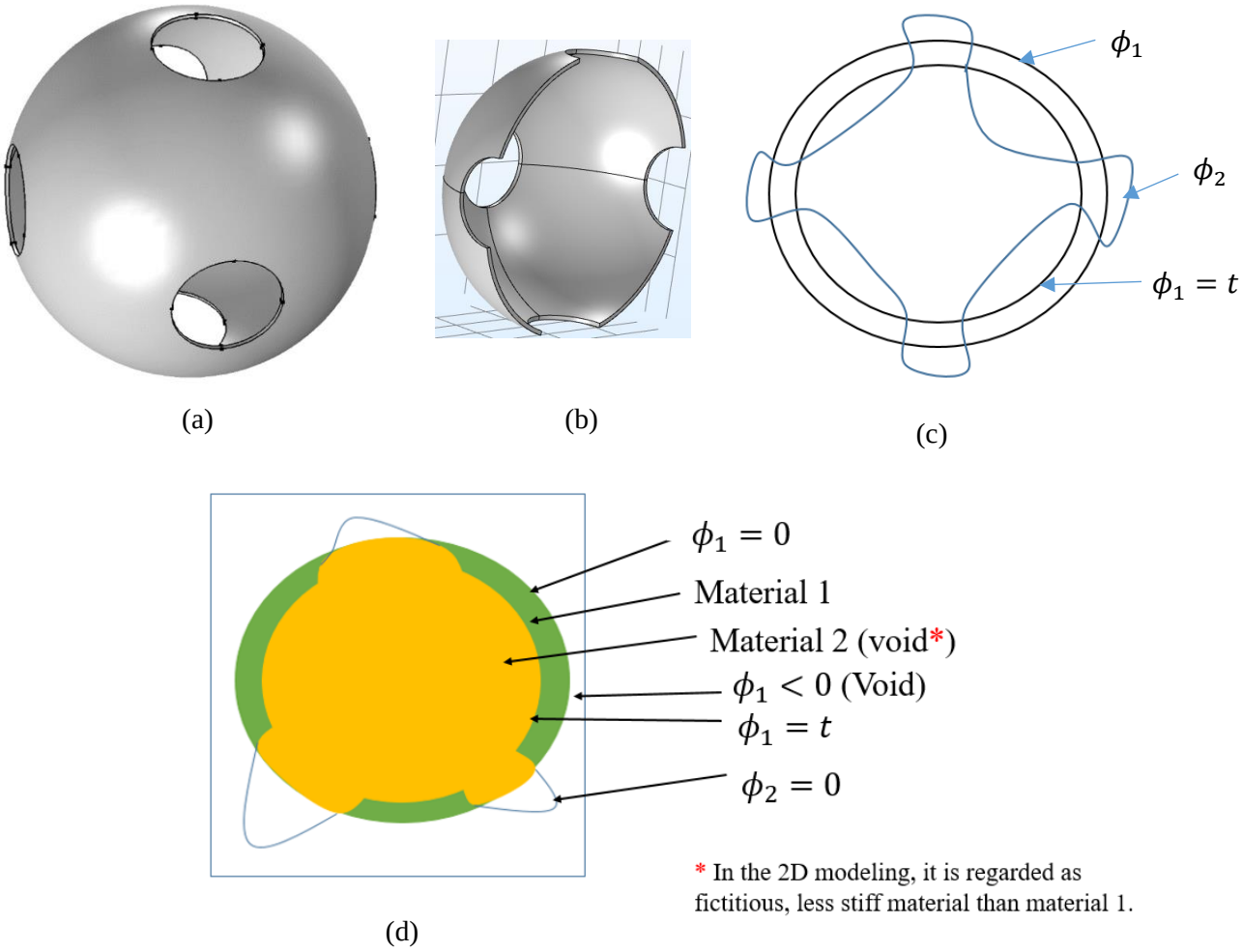

Figure 4. 3 (a) Monolithic TWS (b) Half of monolithic TWS (c) Level set representation of monolithic TWS and (d) distributions of materials in 2D modeling of TWS

The material distribution is represented as:

$$\begin{cases} (0 \le \phi_1 \le t) \wedge (\phi_2 < 0) & Material\ 1 \\ (t < \phi_1) \vee ((0 \le \phi_2) \wedge (0 \le \phi_1) & Material\ 2 \\ (\phi_1 < 0) & Void \end{cases} \tag{4-3}$$

While this representation covers a wide range of thin-walled structural assemblies observed in practice, it should be noted that the geometry with branching walls, such as the one shown in Figure 4.4, cannot be represented. Some of the thin-walled structures have branching walls. This limitation in the formulation will be addressed in the future work.

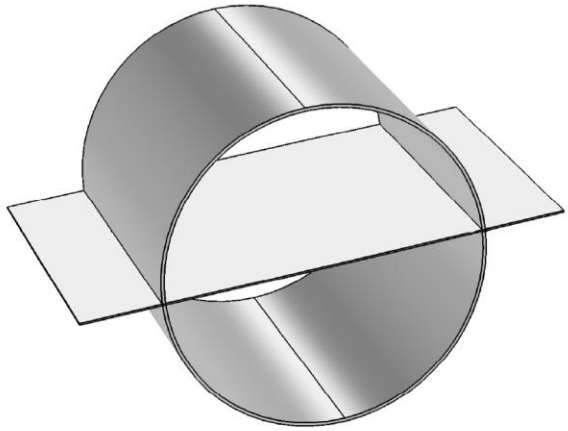

Figure 4. 4 Example of TWS with branching topology

4.3 Representation of multiple materials in topology optimization

Multi-material topology optimization deals with the distribution of various materials within a monolithic design to obtain an optimal structural performance. Different approaches have been proposed to represent different materials such as SIMP-based method ([122], [98]) and level set method ([30], [107]). Multimaterial representation based on level set includes color level set

model, in which m level set is used to represent 2^m materials including the void [99]; multi-material level set topology description model, in which m level set is used to describe m materials and void [32]; piecewise constant level set model, in which an indicator function is used to identify all the material interfaces by partitioning the design domain into different regions based on different values of the piecewise constant level set [28]. These representations all have their biases or drawbacks which makes them not suitable for the representation of multiple components in TWS. These include difficulties associated with the substitution of the different materials during the computational processes; possibilities of having redundant materials emerge in the design domain; a need to incorporate non-overlap constraints to avoid overlap between each two materials.

4.4 Representation of multiple components in TWS

Two level set functions, ϕ_1 and ϕ_2 are used to represent the base component (monolithic thin-walled structure) while the interactions of additional *k* level set functions, ϕ_3, ϕ_4, …, ϕ_{k+1} and ϕ_{k+2} with the base component gives component 1, component 2, ... and component *k* respectively. A monolithic TWS and corresponding four-component partition of TWS example are illustrated in the Figure 4.5 for 2D and 3D:

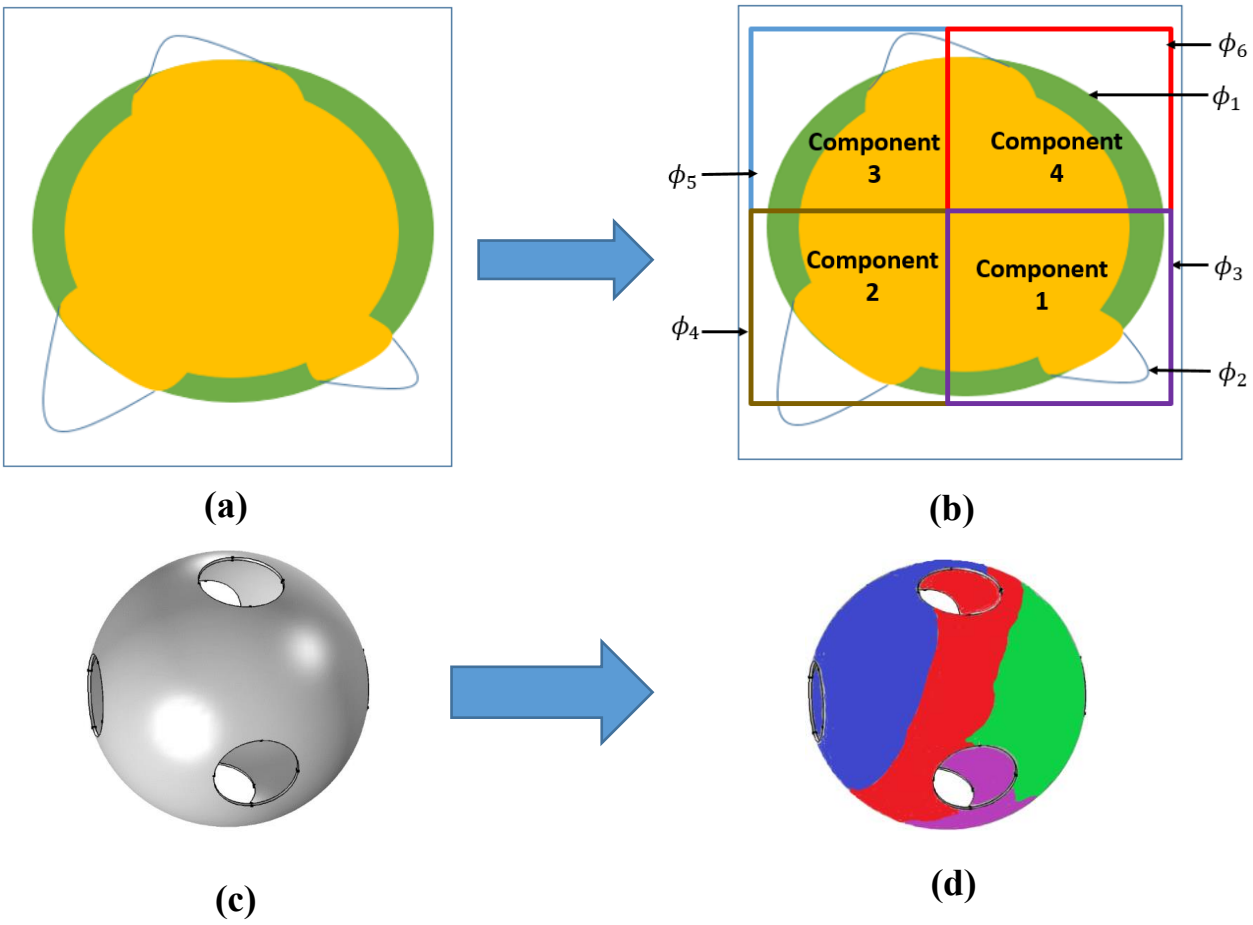

Figure 4. 5 (a) 2D Monolithic TWS (b) Four-component TWS in 2D (c) 3D Monolithic TWS (d) Four-component TWS in 3D

Mathematical modeling of level set-based MTO (LMTO) for TWS is described in Figure 4.5. The dominating base level set for the base component of TWS is ϕ_1 (ϕ_2 is only used to cut holes on ϕ_1). That means the interaction of component level set with ϕ_1 is sufficient for the geometrical modeling of multicomponent TWS (Figure 4.6). Note however that in the sensitivity computation and finite element analysis, all level sets are required – this geometrical description is just for simplification purposes to make explanation easier and straightforward. The actual TWS partitioning is as shown in Figure 4.5.

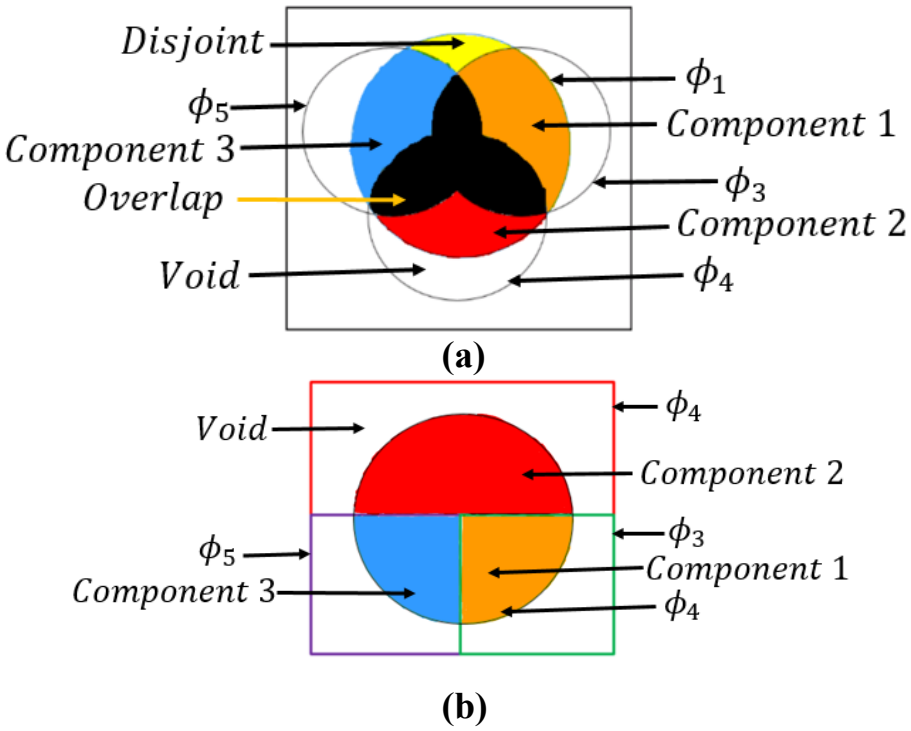

Figure 4. 6 Simplified Three-component TWS, excluding ϕ_2 (a) Base level set interacting with component level sets including overlaps (b) With Equality constraint satisfied

$$\begin{cases} (\phi_1 \geq 0) \wedge (\phi_3 \geq 0) \quad Component\ 1\ (Orange) \\ (\phi_1 \geq 0) \wedge (\phi_4 \geq 0) \quad Component\ 2\ (Red) \\ (\phi_1 \geq 0) \wedge (\phi_5 \geq 0) \quad Component\ 3\ (Blue) \\ (\phi_1 < 0) \wedge (\phi_3 < 0) \wedge (\phi_4 < 0) \wedge (\phi_5 < 0)\ Void\ (White) \end{cases} \tag{4-4}$$

Overlap regions of level sets (black region)

$$\begin{cases} (\phi_1 \geq 0) \wedge (\phi_3 \geq 0) \wedge (\phi_4 \geq 0) \\ (\phi_1 \geq 0) \wedge (\phi_3 \geq 0) \wedge (\phi_5 \geq 0) \\ (\phi_1 < 0) \wedge (\phi_4 \geq 0) \wedge (\phi_5 \geq 0) \end{cases} \tag{4-5}$$

ϕ_1 region that does not interact with any of ϕ_3, ϕ_4 and ϕ_5 , the ‘disjoint region” (Yellow region)

$$(\phi_1 \geq 0) \wedge (\phi_3 < 0) \wedge (\phi_4 < 0) \wedge (\phi_5 < 0) \tag{4-6}$$

Overlapping regions of two or more component level sets is assigned a weak material properties to discourage such regions during optimization. Similar treatment is given to ϕ_1 region that does not interact with any of ϕ_3, ϕ_4, and ϕ_5, that is, the disjoint region. In this formulation, each of the level set functions interacts with the base level set ϕ_1 to give a component.

Thanks to the equality constraint:

$$H(\phi_3) + H(\phi_4) + H(\phi_5) = 1 \quad (4\text{-}7)$$

Where H is the Heaviside function as defined in [104]

At convergence, the component level sets (in this illustration, ϕ_3, ϕ_4, and ϕ_5) fill the design domain. Although the derivation is based on three-component, the application of the proposed formulation to n–component framework is straightforward, and n–component TWS just requires $n + 2$ level sets in total. That is, two level sets to define the based TWS and n additional level sets to partition the base TWS to n components.

4.5 Manufacturability constraints

It is assumed that the components are manufactured by stamping sheet metals of a prescribed thickness. Based on [73], simplified according to [52], the cost of sheet metal stamping consists of die-set cost and die machining cost. The die-set cost of each component is modeled as the minimum-area bounding box (MABB) of the component and the die-machining cost is modeled as the length of the perimeter of the component as illustrated in Figure 4.7. However, because of the difficulty inherent boundary-to-boundary differentiation in level set framework, the perimeter constraint is not included in this present formulation. The dimension of the MABB is approximated with p-norm for ease of differentiation.

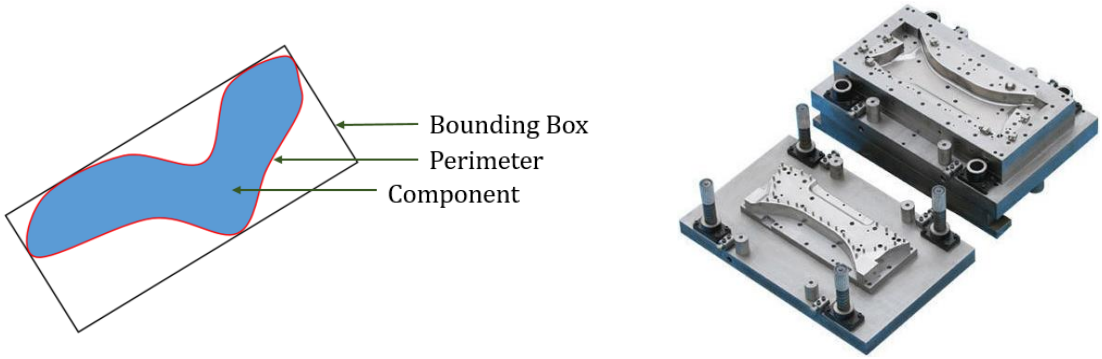

Figure 4. 7 (a) Bounding box and Perimeter of a component (b) Die set for stamping

Constraint on the size of the bounding box for each component is given as:

$$A_h \leq A_h^* \tag{4-8}$$

$$A_h = \prod_{j=1}^{n} l_{j_h} \tag{4-9}$$

$$l_{j_h} = 2\left(\frac{1}{N}\sum_{i=1}^{N} \rho_{i_h}(z_{ji_h} - c_{j_h})^p\right)^{\frac{1}{p}} \tag{4-10}$$

$$c_{j_h} = \frac{\sum_{i=1}^{N} \rho_{i_h} z_{ji_h}}{\sum_{i=1}^{N} \rho_{i_h}} \tag{4-11}$$

$$\rho_{i_h} = \begin{cases} 0 & \text{if element } i \text{ belongs to void region } (\phi_1 < 0) \\ 1 & \text{otherwise} \end{cases}$$

where A_h is the MABB for component h that approximates the die-set cost; A_h^* is the maximum allowable area that approximates maximum allowable die-set cost for component *h*; *n* is the number of dimensions in design domain (*n* = 2 for 2D and n= 3 for 3D); l_{j_h} is the *p*-norm approximated dimension of component *h*; ρ_{i_h} is a binary variable indicating the existence of

materials in element i in component h; z_{ji_h} is the j-th coordinate of the center of each element i of component h; and c_{j_h} is the j-th coordinate of the center of the component h.

While not directly related to manufacturability, the total material cost of the structure is accounted in the form of constraint on the total volume of the component, given as

$$V \leq V^* \tag{4-12}$$

where V^* is the maximum allowable volume of TWS and V is the estimated volume of the base TWS.

4.6 Shape derivative

Due to its computational efficiency, a gradient-based optimization algorithm is used for optimizing the multi-component thin-walled structural topology represented by ϕ_1 and ϕ_2, …, $\phi_{2+\mathrm{k}}$. In this research, the shape derivatives are used as the gradient, due to their relative simplicity in implementation. The shape derivative of a function with respect to a level set is defined as the change in the function value as a result of the infinitesimal change in the leveled boundaries. In the context of structural optimization, therefore, the shape derivative can only drive the changes in the boundary shape, not topology, of structures. While topological derivatives can change the boundary topology (i.e., create holes) during optimization, the effect can be approximated by the merging of the holes introduced at the initialization, as commonly done in the previous work ([35], [37], [104]).

Dissimilar to solid structures that have only two domains (material or void), the proposed representation of the monolithic thin-walled structure (a pair of closed offset surfaces with holes) consists of three distinct domains: material 1 defined by $(0 \leq \phi_1 \leq t) \wedge (\phi_2 < 0)$, shown in green, material 2 defined by $(t < \phi_1) \vee ((0 \leq \phi_2) \wedge (0 \leq \phi_1))$, shown in yellow, and void

defined by $\phi_1 < 0$, shown in white in Figure 4-3 (c). This serves as the base component. Each of these is separately taken into account in the derivation of the shape derivative. The detailed derivation of the shape sensitivities are included in Appendix A.

4.7 Optimization model

The overall optimization model can be formulated as:

$$min: compliance(\phi_1, \phi_2, \dots \phi_{2+k}) \qquad (4-13)$$

$$subject\ to:$$

$$V(\phi_1, \phi_2) \leq V^*$$

$$A_h \leq A_h{}^*$$

$$\sum_{h=1}^{K} H(\phi_{h+2}) = 1$$

where $compliance$ is the objective function. Compliance is expressed as this summation of the absolute maximum displacement for each loading condition for the multi-loading problem. For single loading problem, the compliance is expressed as the product of the applied force and absolute maximum displacement. Since thin-walled structures are hypothetically modeled as 2D planar structure in the following numerical examples, the total volume of the base TWS is approximated as $V_2 + \frac{rV_1}{t}\sqrt{V_2}$, in order to account for the volume of thin-walls in z-direction.

4.8 Optimization algorithm

The finite element analysis is implemented in Comsol Multiphysics while the level set functions are updated using gradient-based optimization algorithms in [104].

4.9 Case studies conducted for the 2D modeling

This section discusses the case studies used for several examples based on the 2D implementation of the mathematical formulation presented in this Chapter. Figure 4.8(a) illustrates the 2D representation of an example monolithic TWS defined by ϕ_1 and ϕ_2. The resulting 2D geometry is a closed, simply-connected region shown in gray, outlined by the (possibly disconnected) strips with a small constant thickness shown in blue. Figure 4.8(b) illustrates an example partitioning of the monolithic TWS into 4 components.

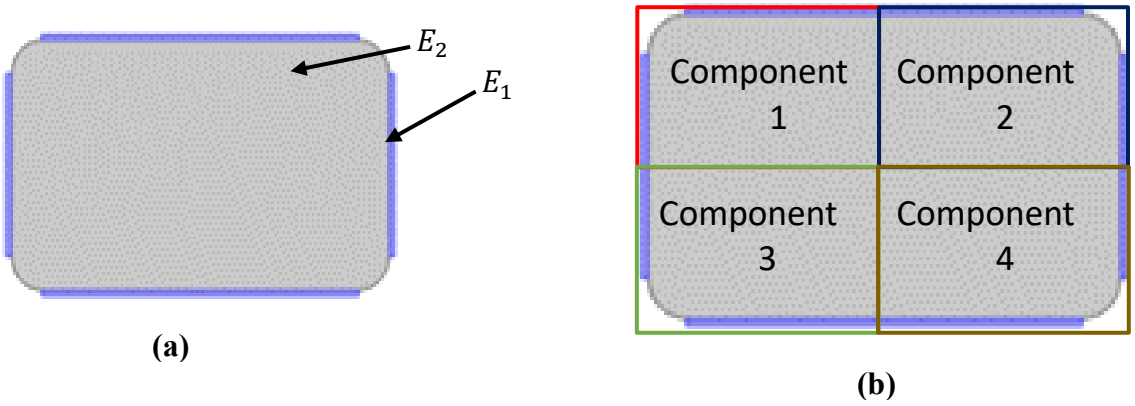

Figure 4. 8 (a) 2D representation of geometry represented by ϕ_1 and ϕ_2 and (b) its four-component partitioning

In 3D, this gray region represents the internal void of the closed surface represented by ϕ_1. However, this cannot be the case for the 2D counterpart, because very low stiffness (= void) in the gray region would cause any geometry with disconnected outlines to have singular stiffness matrix. This singularity is avoided by modeling the gray region with a "substrate" material, which approximates the 3D surface that exist "behind" the plane on which the 2D design domain is defined. Then, the stiffness of the gray region, E_2 is comparable but no higher than the one of the thin strips, E_1. In the examples presented in the following subsections, the value of E_2 was set as 70% of E_1, based on the examinations of representative 3D sheet metal parts and their 2D

equivalents (Appendix B). Despite its analogy to 3D counterpart, however, no hole can exist in the gray region during optimization.

Two structures are used to demonstrate the viability of the formulation, as shown in Figure 4.9. The input parameters common to both examples are summarized in the Table 4. 1. Unitless values are used in the examples because they are linear elastic problems. The finite element analysis is done in Comsol Multiphysics and the simulation is done in MATLAB (by Mathworks). The 2 by 1 design domain is discretized into 80 by 40 (3200) linear elements. This is carried out on a standard desktop PC (CPU: Xeon E3-1241 v3 3.5GHz; RAM: 16 GB)

Table 4. 1 Input parameters used in examples

Parameter	Values	Description
E_1	3	Young's modulus for material 1
E_2	$0.7E_1$	Young's modulus for material 2
E_0	10^{-3}	Young's modulus for the void region

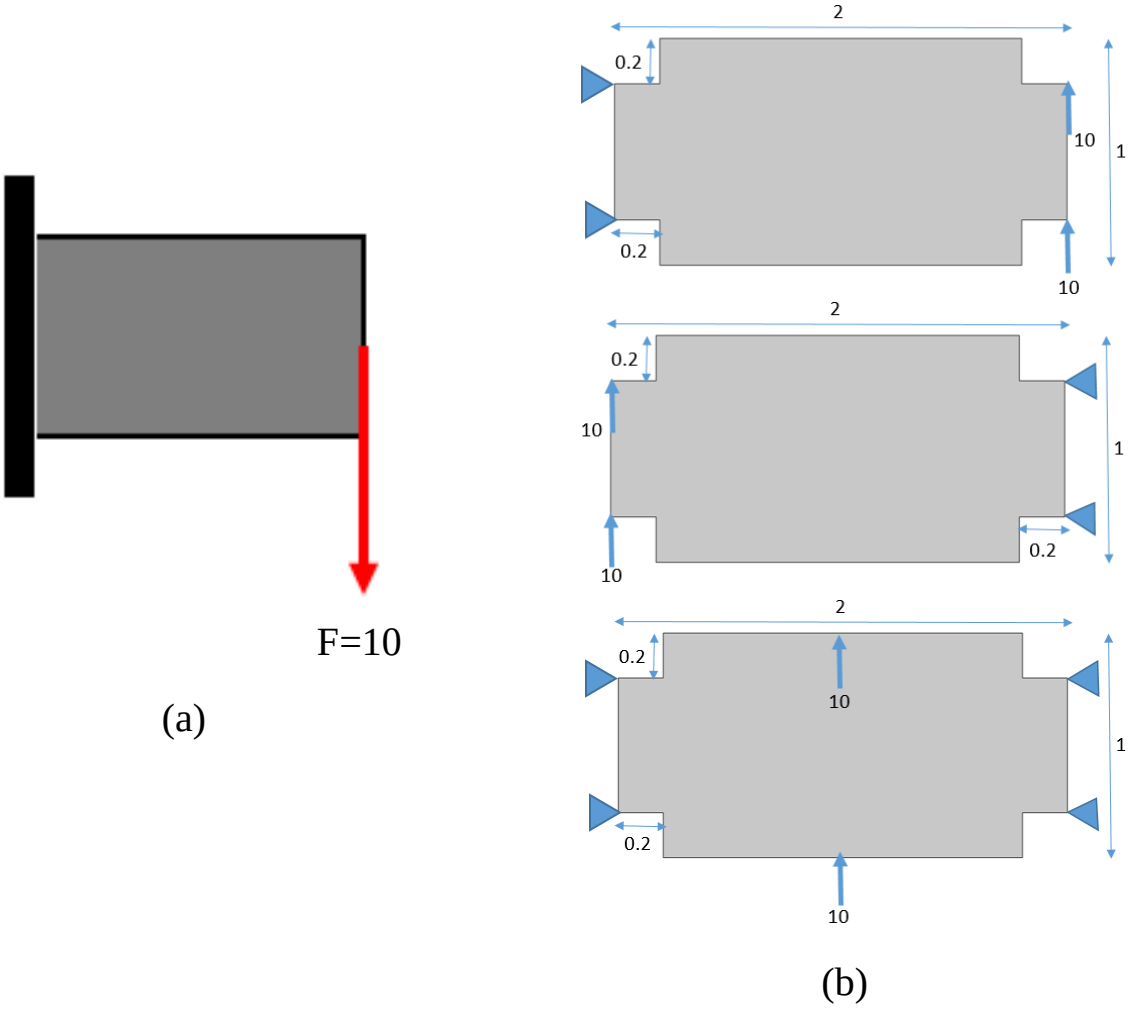

Figure 4. 9 (a) 2 by 1 Cantilever. (b) Simplified automotive floor frame subject to multiple loading

CHAPTER 5

Numerical Results

5.1 Example 1

5.1.1 Example 1.1: 4-component TWS Cantilever (Symmetrical initialization)

A 2 by 1 cantilever, fixed at the left end and with a downward force of 10 applied at the midpoint on the right end is implemented (Figure 4.9(a)).

For this example, $r = 0.3$ and $t = 0.05$. Table 5.1 gives the required parameters, initialization and the optimized results. The initialization is symmetrical since the intention is to have a symmetrical convergence. The optimization started with a feasible design. Compliance which is the objective is defined here as the product of maximum absolute displacement and absolute force applied. The compliance at the initialization was high. Since the volume constraint and manufacturing constraints were not active initially, the optimizer attempt to decrease the compliance in the early iteration while sacrificing the volume and mabb, driven by compliance sensitivity. Once the volume constraint reached the set value, the optimizer continued by minimizing the compliance objective, while sacrificing the mabb, driven by compliance sensitivity until the compliance objective was reached. At convergence, the volume constraint V and the mabb for components 1 and 3, A_1 and A_3 were active while mabb for component 2 and 4, A_2 and A_4 were not active. This shows that for the prescribed material cost, the manufacturing cost set for component 1 and 3 are appropriate while the manufacturing cost set for component 2 and 4 are in excess. Figure 5.2 to

5.4 show the initializations of level set, material, component and mabb, while Figure 5.5 to 5.7 show their corresponding optimization results. Figure 5.8 shows the convergence history of the optimization.

Table 5. 1 4-component TWS Cantilever (Symmetrical initialization)

Parameter	Required	Initial	Optimization result
$Compliance$		$5.8 * 10^5$	$1.1 * 10^4$
V	0.6	0.03	0.6
A_1	0.065	$1.4 * 10^{-3}$	0.063
A_2	0.065	$2 * 10^{-3}$	0.044
A_3	0.065	$2 * 10^{-3}$	0.065
A_4	0.065	$1.4* 10^{-3}$	0.061

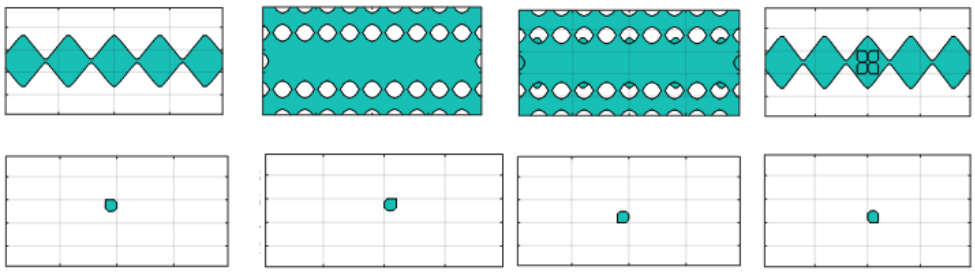

Figure 5. 1 Initialization of the level sets. From left to right. First row, then second row. ϕ_1; ϕ_2; ϕ_1 and ϕ_2; ϕ_1 and ϕ_3 – ϕ_6; ϕ_3; ϕ_4; ϕ_5; and ϕ_6.

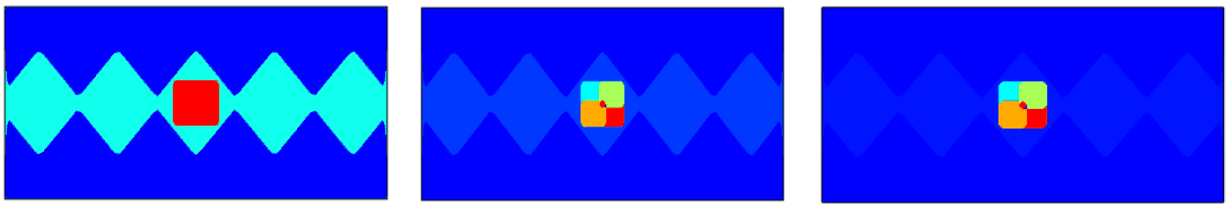

Figure 5. 2 From left to right, Initialization for (a) Material property (b) Component mapping (c) 4-Component TWS

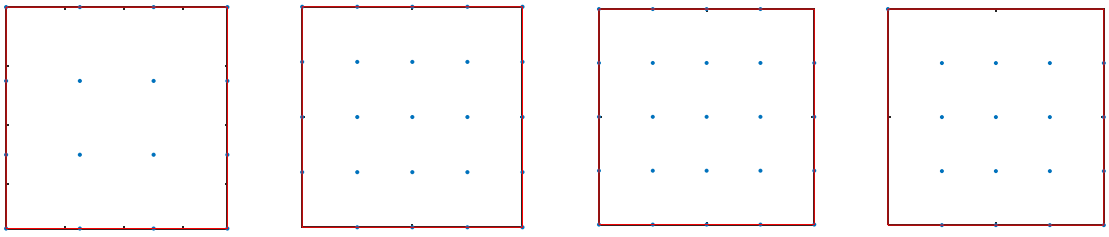

Figure 5. 3 From left to right. MABB for the components 1 – 4

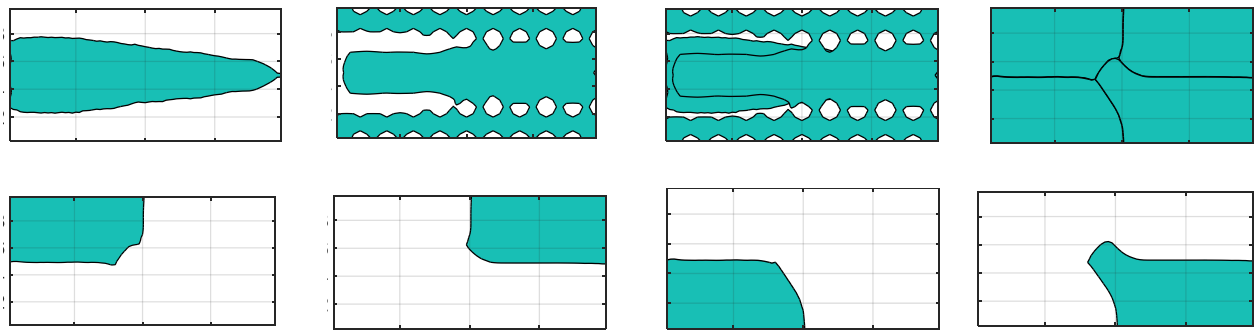

Figure 5. 4 Optimization result of the level sets. From left to right. First row, then second row. ϕ_1; ϕ_2; ϕ_1 and ϕ_2; ϕ_1 and $\phi_3 - \phi_6$; ϕ_3; ϕ_4; ϕ_5; and ϕ_6

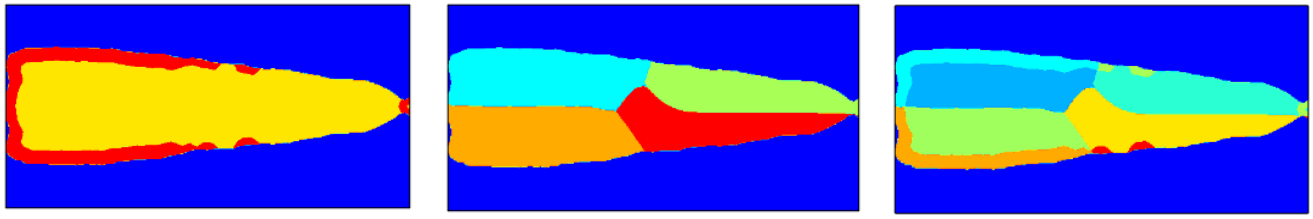

Figure 5. 5 From left to right, Optimization result for (a) Material property (b) Component mapping (c) 4-Component TWS

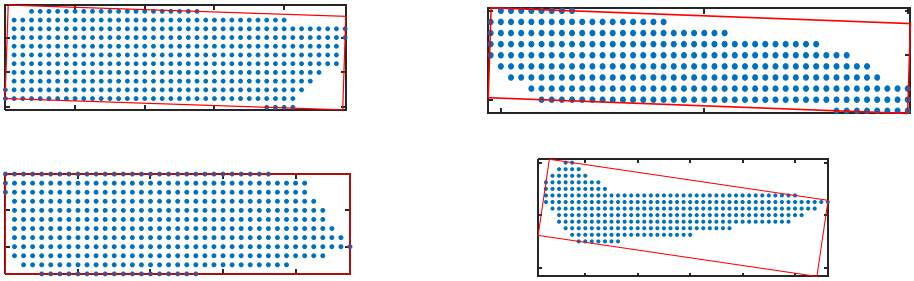

Figure 5. 6 From left to right. First row, then second row. MABB for the optimization result for Component 1 – 4

Figure 5. 7 4-component TWS Cantilever (Symmetrical initialization) convergence history

5.1.2 Example 1.2: 4-component TWS Cantilever (with asymmetrical initialization)

Similar to Example 1, $V = 0.6$, $r = 0.3$ and $t = 0.05$. Table 5. 2 gives the required parameters, initialization and the optimized results. However, required mabb for each component are not the same as Example 1. Compliance which is the objective is defined here as the product of maximum absolute displacement and absolute force applied. The goal of this experiment is to study the optimization and convergence when the initialization is asymmetrical. Figure 5.9 to 5.11 gives the details of the initialization and Figure 5.12 to 5.14 gives the optimization result. Figure 5.15 gives the convergence history. The optimization process is similar to the one described in Example 1.1 However, the optimized structure is asymmetrical. A lesson from this example is that asymmetrical initialization will likely converge to asymmetrical optimized result.

Table 5. 2 4-component TWS Cantilever (Asymmetrical initialization)

Parameter	Required	Initial	Optimization result
$\boldsymbol{Compliance}$		$4.96 * 10^5$	9203
$\boldsymbol{V}$	0.6	0.069	0.6
$\boldsymbol{A_1}$	0.14	0.0056	0.049
$\boldsymbol{A_2}$	0.14	0.0058	0.14
$\boldsymbol{A_3}$	0.14	0.0059	0.021
$\boldsymbol{A_4}$	0.14	0.0035	0.078

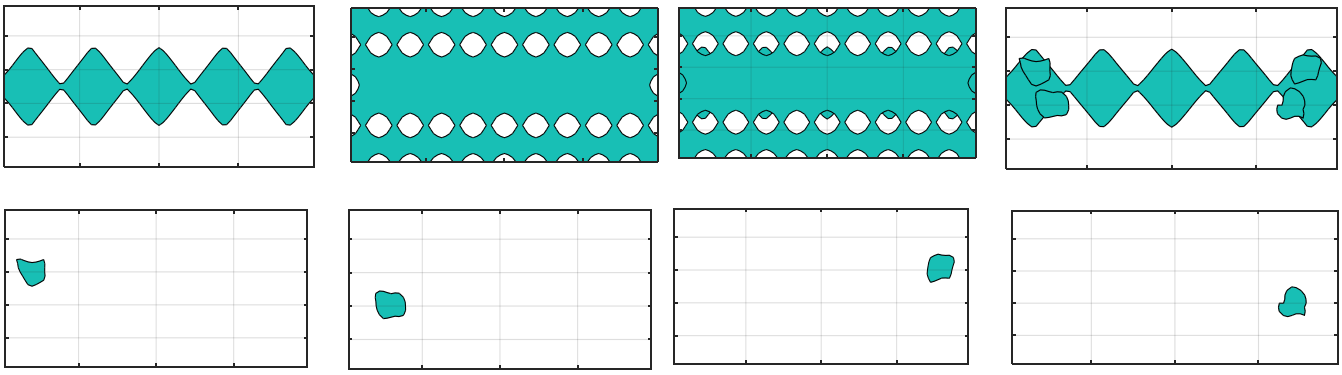

Figure 5. 8 Initialization of the level sets. From left to right. First row, then second row. $\boldsymbol{\phi_1}$; $\boldsymbol{\phi_2}$; $\boldsymbol{\phi_1}$ and $\boldsymbol{\phi_2}$; $\boldsymbol{\phi_1}$ and $\boldsymbol{\phi_3}$ − $\boldsymbol{\phi_6}$; $\boldsymbol{\phi_3}$; $\boldsymbol{\phi_4}$; $\boldsymbol{\phi_5}$; and $\boldsymbol{\phi_6}$.

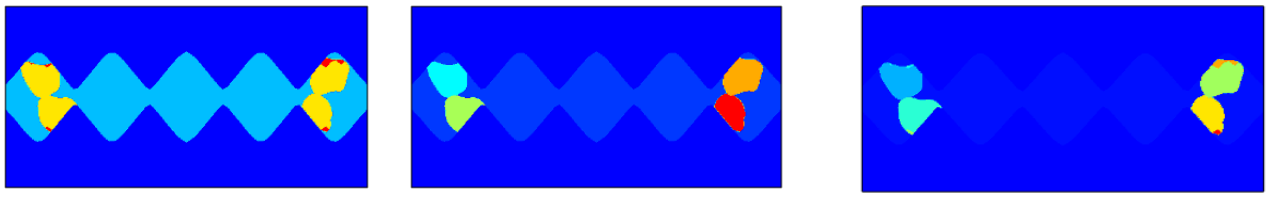

Figure 5. 9 From left to right, Initialization for (a) Material property (b) Component mapping (c) 4-Component TWS

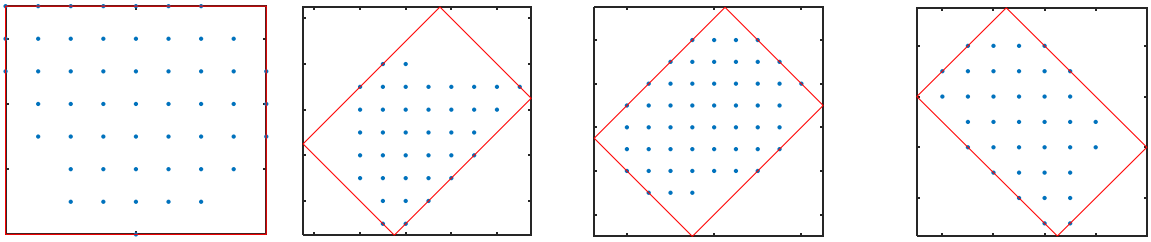

Figure 5. 10 From left to right. Initialization of MABB for the components 1 – 4

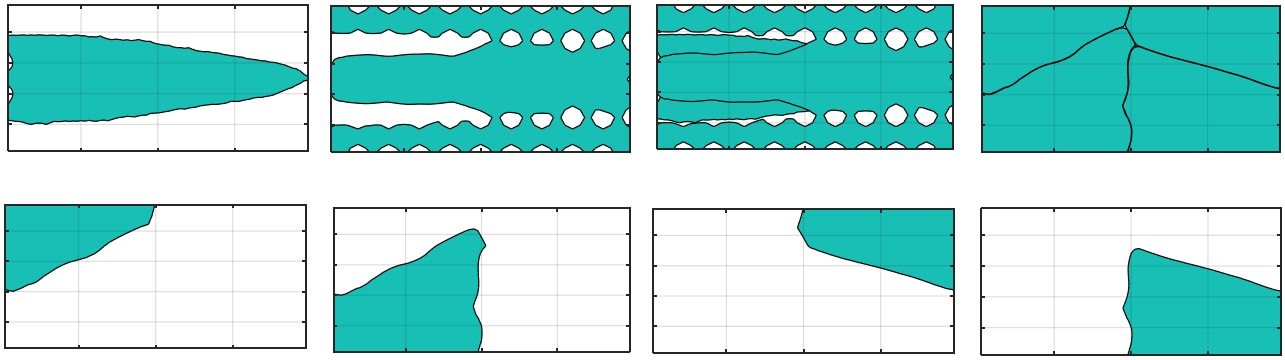

Figure 5. 11 Optimization result of the level sets. From left to right. First row, then second row. ϕ_1; ϕ_2; ϕ_1 and ϕ_2; ϕ_1 and $\phi_3 - \phi_6$; ϕ_3; ϕ_4; ϕ_5; and ϕ_6.

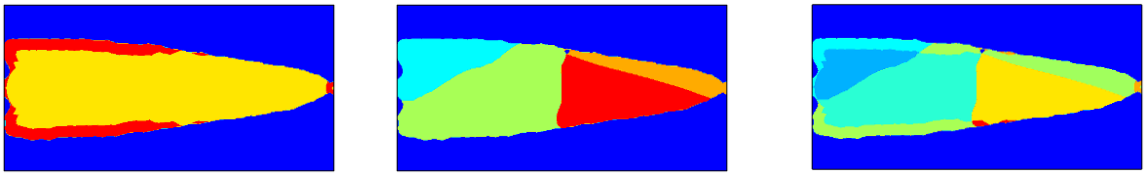

Figure 5. 12 From left to right, Optimization result for (a) Material property (b) Component mapping (c) 4-Component TWS

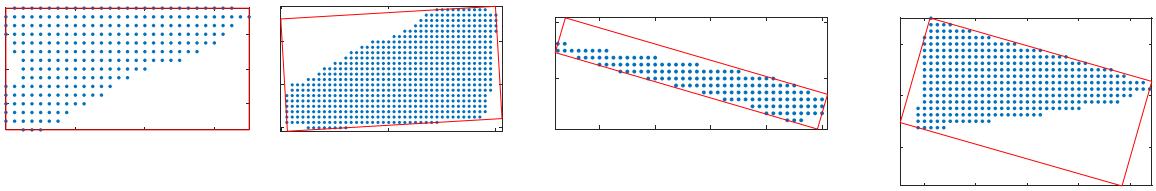

Figure 5. 13 From left to right. MABB for the optimization result for Component 1 – 4

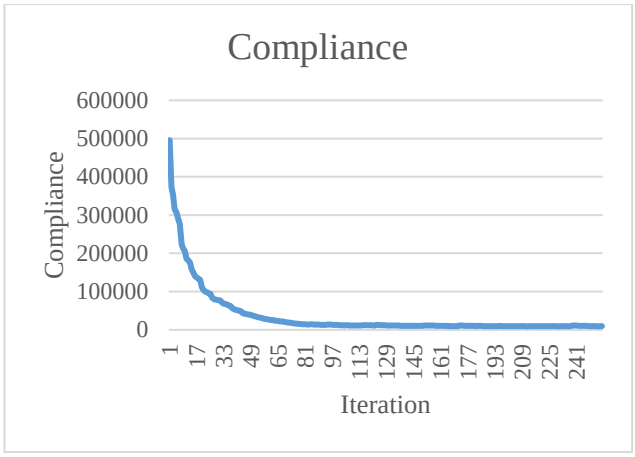

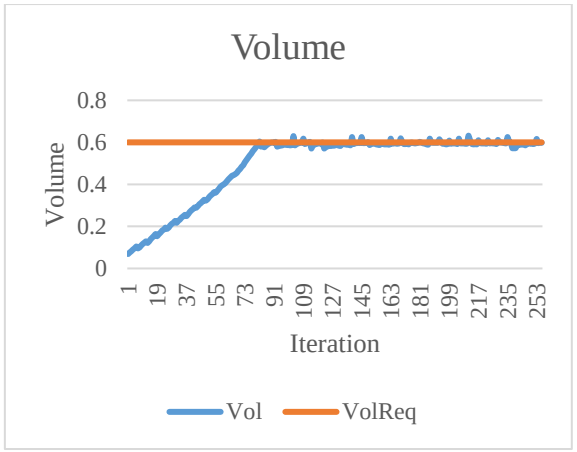

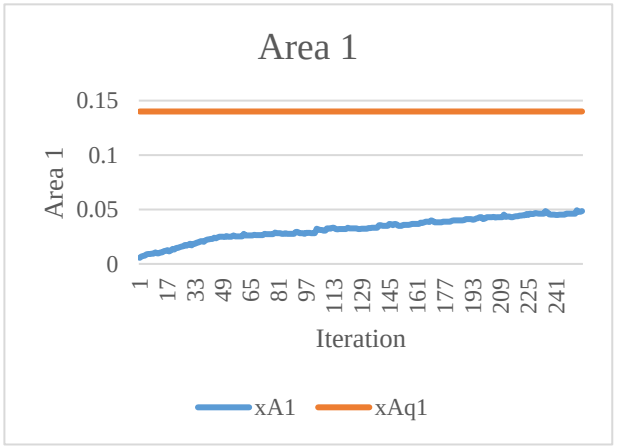

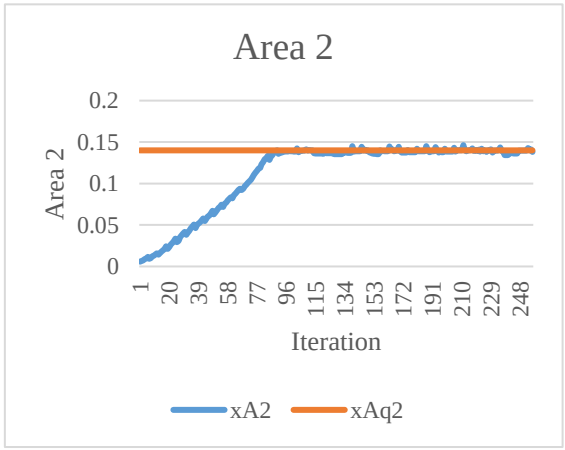

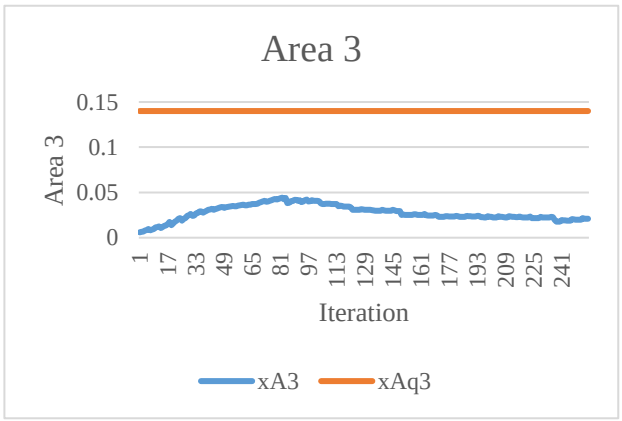

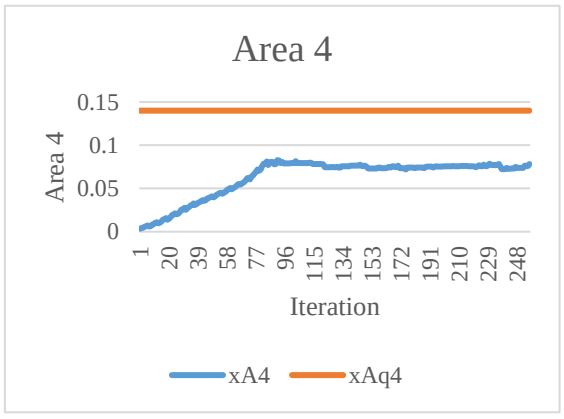

Figure 5. 14 4-component TWS Cantilever (Asymmetrical initialization) convergence history

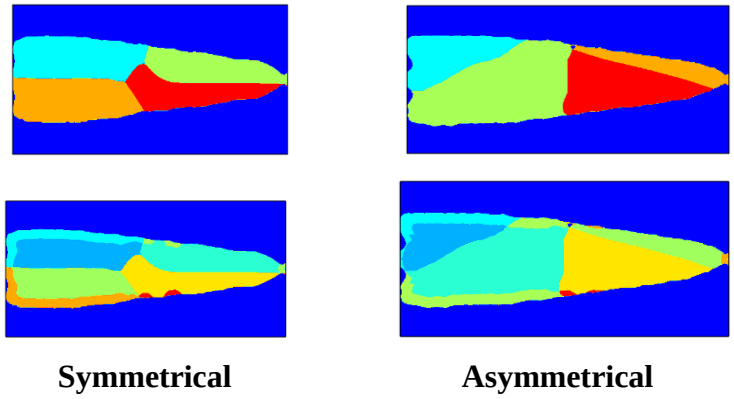

Figure 5. 15 Comparison between Symmetrical and Asymmetrical Initialization for the 4-component cantilever

Table 5. 3 Comparison of optimization results of symmetrical and asymmetrical 4-component cantilever TWS

Parameter	Symmetrical	Asymmetrical
Material cost (***V***)	0.6	0.6
Total ***A***	0.23	0.286
Initial Compliance	$5.8 * 10^5$	$4.96 * 10^5$
Final Compliance	$1.0 * 10^4$	$9.2 * 10^3$

Table 5. 3 gives the comparison between the result for symmetrical and asymmetrical 4-component designs for cantilever TWS (Figure 5.16). Compliance which is the objective is defined here as the product of maximum absolute displacement and absolute force applied. The percentage difference of the two compliance is about 8 percent. This is considered an insignificant difference, possibly results from numerical approximation during simulations. There is therefore no influence of the total manufacturing cost on the compliance. This is because there is no joint. The result indeed shows that the compliance of the asymmetrical and symmetrical design are similar. Incorporation of joint in the future work may lead to a different result for this kind of experiment.

The effect of initialization for partitioning is primarily due to the fact the current formulation does not have joint – so the optimizer simply grows each component level set from the initial position/size until either it hits another component level set and/or satisfy the prescribed mabb

specified for the component it represents. Without joint, basically two-step process will produce the same result as in this formulation. So, the sensitivities of the component level sets are not due to the optimizer. On the other hand, initialization of $\boldsymbol{\phi_1}$ affects the converged $\boldsymbol{\phi_1}$ shape, which is due to local optima. It is expected theoretically that if the optimization is repeated infinite number of times with all possible initializations, there is possibility of achieving a global optimum. However, since this is not easy to implement, "acceptable" initialization is based on the number of factors such as desire for symmetry and the imposed manufacturability constraints.

5.1.3 Example 1.3: Representation of arbitrary numbers of components

The proposed formulation can also represent arbitrary number of components. Some of the issues in the definition of multiple phases have been addressed in this formulation. The formulation can be used to design any arbitrary number of components. This is much easier to implement, since each component partition is represented strictly by a level set. Also, this formulation can eliminate components in the process of optimization. Therefore, the constraints can be placed on the maximum number of components to which the optimization should converge. That interesting capability of this formulation to constrain the maximum number of components, regardless of the number of components at the initialization will be implemented in the future work. This dissertation however demonstrates the capacity of the formulation to design multiple components. Table 5. 4 shows the parameters for the cases (one-component to four-component) that are demonstrated. Figure 5. 17 gives the representation of those cases.

Table 5. 4 Parameters for the number of components implemented for a cantilever TWS

Number of components	V	$Max\ A$ for each component	*Final Total A*	r	t	Compliance
1	0.50	0.550	0.55	0.05	0.05	4133
2	0.50	0.255	0.426	0.05	0.05	4178
3	0.50	0.220	0.418	0.05	0.05	4160
4	0.50	0.11	0.340	0.05	0.05	4227

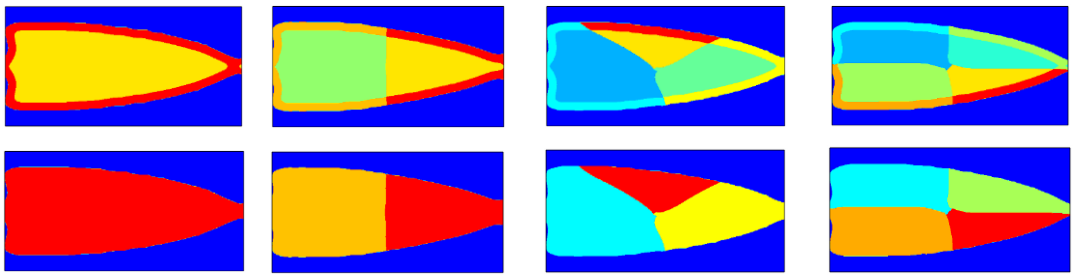

Figure 5. 16 Representation of arbitrary number of components. From left to right. 1-component to 4-component. Row 1 shows the n-component TWS. Row 2 shows the partition into various components

The proposed formulation can be used to represent n-component. In this experiment, the same values are used for $V, r,$ and t in all the cases. Compliance for the single-loading problem which is the objective is defined as the product of absolute maximum displacement and absolute applied force. The percentage range difference is about 2 percent. This is considered an insignificant difference among the compliance, possibly results from numerical approximation during simulations. Therefore, there is no influence of total manufacturing cost or number of components on the compliance, since there is no joint. The compliances are indeed similar for all cases.

5.1.4 Example 1.4: Multi-loading problem

In the real word, structures are usually subjected to multiple loading. The capability of the proposed formulation to handle multi-loading problem is examined. A simplified automotive floor frame subject to multiple loading [52] is implemented for 4-component thin-walled structures. Figure 5.3(b) shows the loading condition and Figure 5.18 to 5.24 shows the

initialization, optimization result and convergence history; and Table 5. 5 shows the numerical result. The initialization is symmetrical and the optimization result is fairly symmetrical. The values of r = 0.05 and t = 0.05. At convergence, all constraints are active. Compliance which is the objective is defined here as the sum of the maximum absolute displacement for each of the loading cases. The starting compliance is 1.1 * 10^5 and the final compliance is 3.5 * 10^3. The trend of the optimization is similar to Example 1.1. That is, the compliance is minimizing at the cost of increasing material and manufacturing cost, until the constraints become active, and then convergence is reached, balancing the costs and the compliance objective. This result does not represent the actual loading condition for the automotive floor frame. It is however a simplified form, and the purpose is to demonstrate the application of the proposed formulation in solving multi-loading problem.

Table 5. 5 Multi-loading problem

Parameter	Required	Initial	Optimization result
$Compliance$		1.1 * 10^5	3532.8
V	0.55	0.025	0.55
A_1	0.12	0.0011	0.12
A_2	0.12	0.0015	0.12
A_3	0.12	0.0015	0.12
A_4	0.12	0.0011	0.12

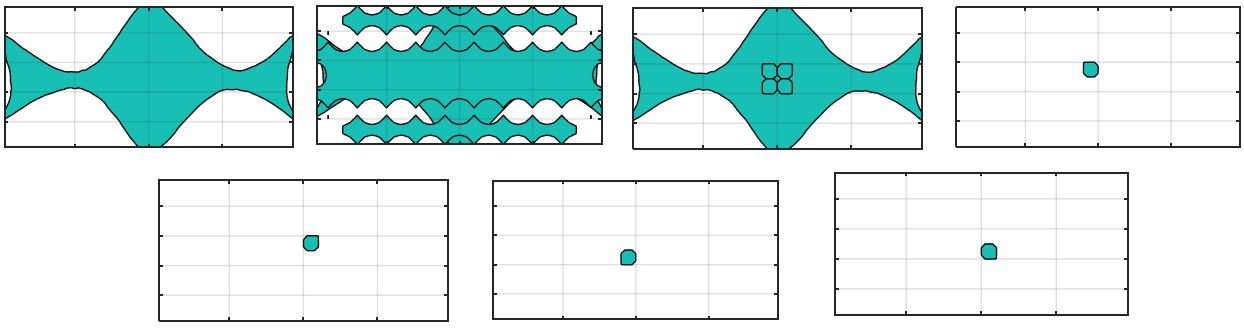

Figure 5. 17 Initialization of the level sets. From left to right. First row, then second row. ϕ_1; ϕ_1 and ϕ_2; ϕ_1 and ϕ_2; ϕ_1 and $\phi_3 - \phi_6$; ϕ_3; ϕ_4; ϕ_5; and ϕ_6

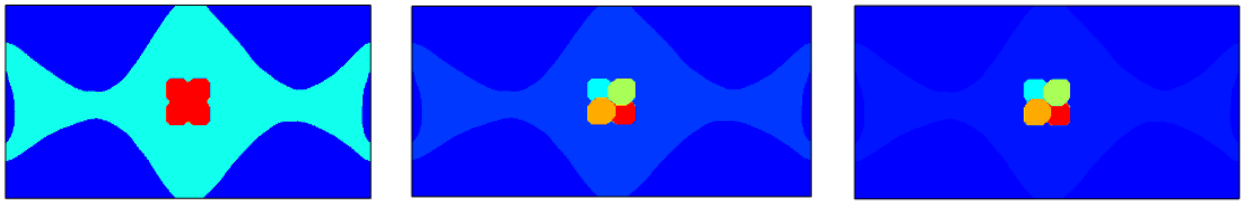

Figure 5. 18 From left to right, Initialization for (a) Material property (b) Component mapping (c) 4-Component TWS

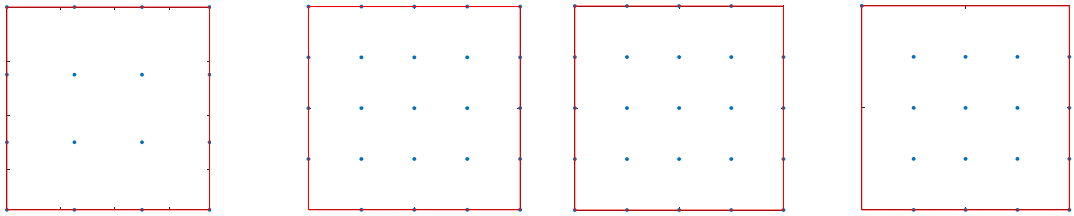

Figure 5. 19 From left to right. Initialization of MABB for the components 1 – 4

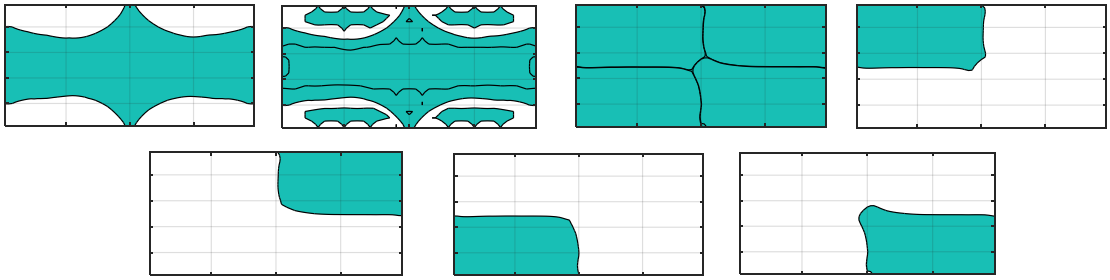

Figure 5. 20 Optimization result of the level sets. From left to right. First row, then second row. ϕ_1; ϕ_1 and ϕ_2; ϕ_1 and ϕ_2; ϕ_1 and $\phi_3 - \phi_6$; ϕ_3; ϕ_4; ϕ_5; and ϕ_6

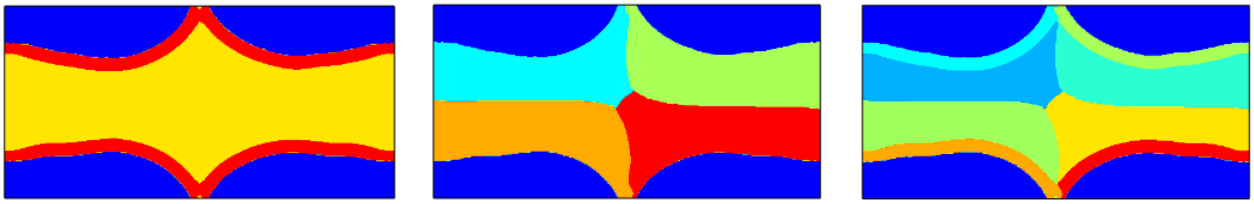

Figure 5. 21 From left to right, Optimization result for (a) Material property (b) Component mapping (c) 4-Component TWS

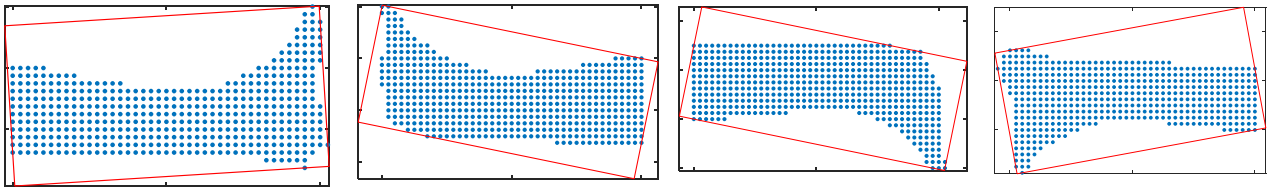

Figure 5. 22 From left to right, then up to down. MABB for the optimization result for Component 1 – 4

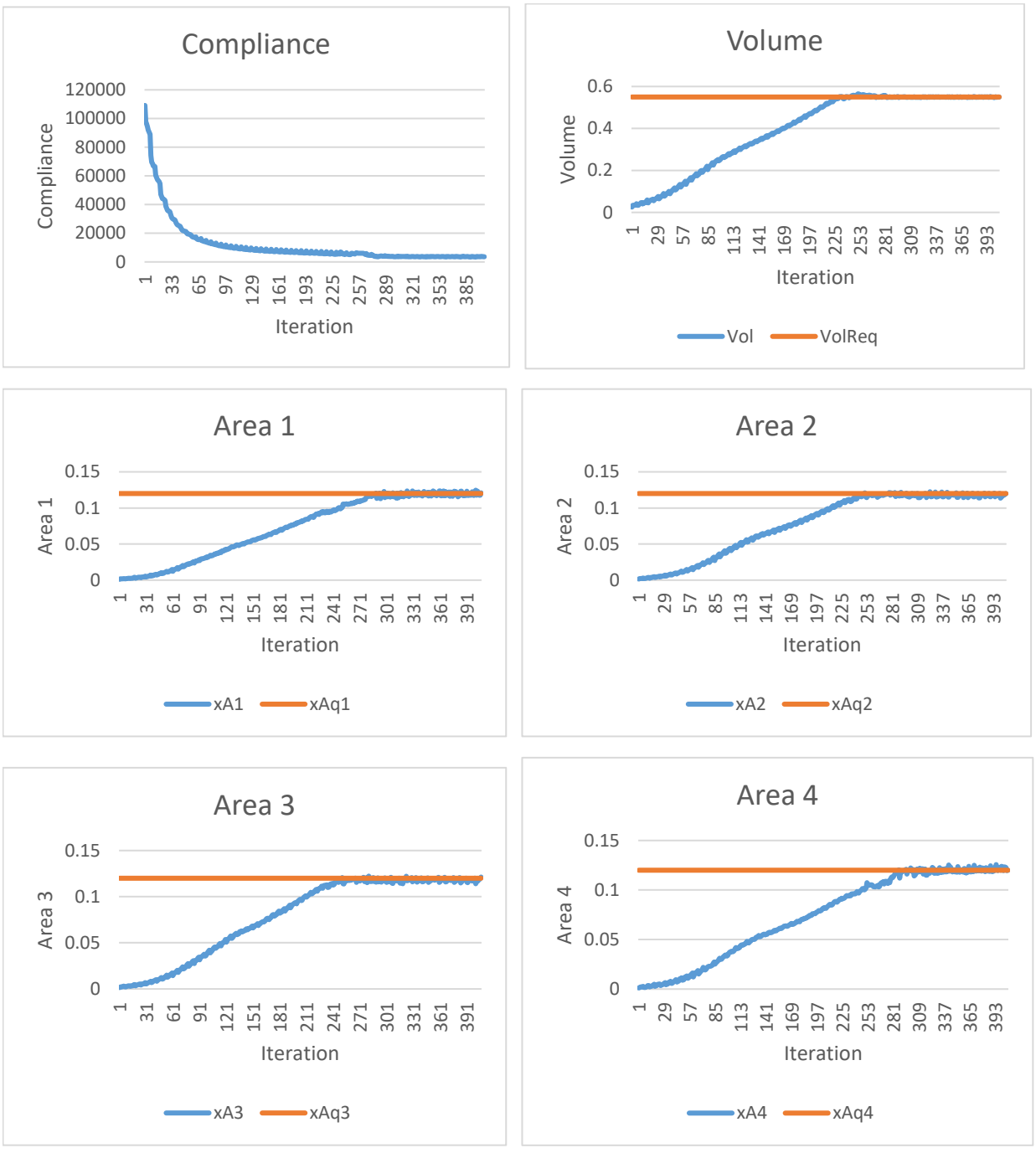

Figure 5. 23 4-component TWS Simplified Automotive Floor Frame under Multiple Loadings convergence history

CHAPTER 6

Preliminary Joint Modelling

6.1 MABB-based joint model

The joint is modeled as the mabb of two component level sets overlap with the constraint on the thickness of the joint (Figure 6.1). The minimum of the two-dimensions gives the thickness of the joint as shown in Equation 6-1. A "fill constraint" is imposed to ensure that the joint substantially fill its bounding box, to guide against incomplete partitioning.

$$t_{joint} = \max_{j=1,2} \frac{1}{l_j} \qquad (6\text{-}1)$$

Where:

$$l_j = 2\left(\frac{1}{N}\sum_{i=1}^{N} \rho_i (z_{ji} - c_j)^p\right)^{\frac{1}{p}} \qquad (6\text{-}2)$$

$$\rho_i = H(\phi_1)H(\phi_3)H(\phi_4) \qquad (6\text{-}3)$$

ρ_i is the density of the joint, l_j is the length of each dimension and t_{joint} is the thickness of the joint. The details of the remaining notations is in Appendix A.

This is a continuous formulation which makes it possible to incorporate the formulation into the gradient-based algorithm. The drawback of this approach is that the joint will always be straight; that means the optimization result cannot produced non-straight joint which is not uncommon in the real-world geometry.

In the 3D formulation, the Young's modulus of elasticity for joint is one value. However, in the current implementation, the joint has two material properties namely: the joint material property E_3 for the shell material region (E_1 region), and the joint material property E_5 for the fictitious material region (E_2 region) (Figure 6-1).

Figure 6.2 gives the examples of LMTO with joint modeling for cantilever and Figure 6.3 gives the corresponding level sets. The material properties are: $E_1 = 3$, $E_2 = 2.1$, $E_3 = 1.43$, and $E_5 = 1$.

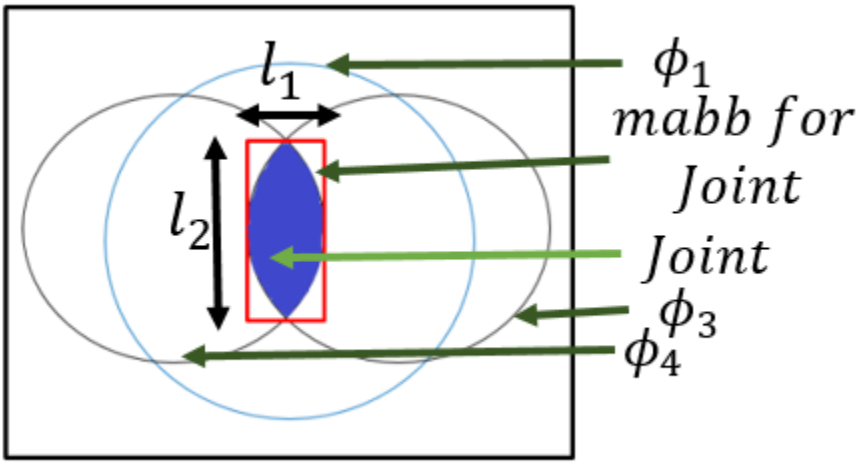

Figure 6. 1 Simplified two-component TWS with joint modeling. ϕ_2 is not included since the purpose of ϕ_2 is to cut holes on ϕ_1

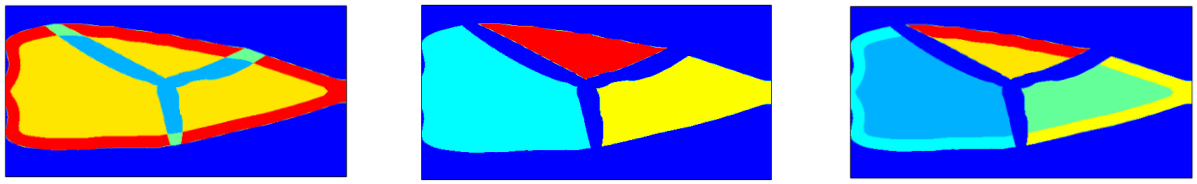

Figure 6. 2 LMTO for TWS with joint modeling for a three-component cantilever in Figure 5-3: (a): ($V = 0.4$; Joint thickness (t_{joint}) = 0.05; MABB for each component = 0.2; and Compliance = 5.4*103)

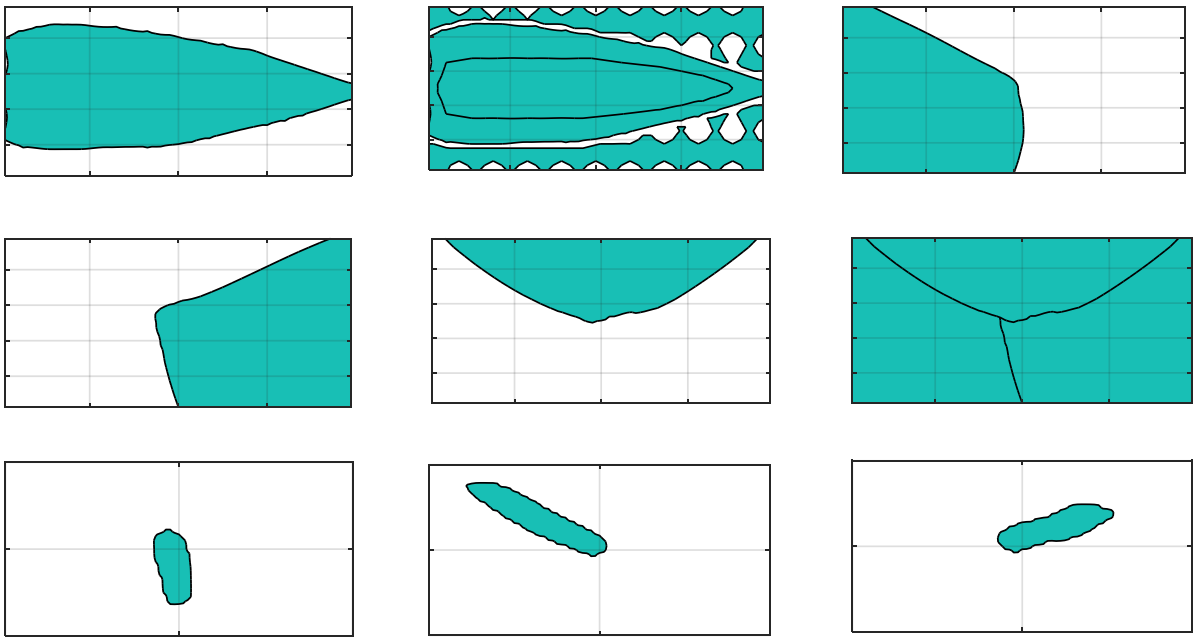

Figure 6. 3 The corresponding level set for the optimization result of Figure 6-2. From left to right. First row: ϕ_1; ϕ_1 and ϕ_2; ϕ_3. Second row: ϕ_4; ϕ_5; $\phi_1, \phi_3 - \phi_5$; Third row: $\phi_3 \Lambda \phi_4$; $\phi_3 \Lambda \phi_5$; $\phi_4 \Lambda \phi_5$

A better approach for joint modeling would be to directly model the joint as the boundary-to-boundary point of contacts of two or more level set. The equality constraint ensures that there is no level set overlap. The specification of the joint width is then straightforward, as that is defined as the linear function of the width assigned to the boundaries of the level sets defining the components. This is similar to the two pieces of TWS brought together to join with welding at the contact points. The width of the joint is the twice the width of the boundary of a level set. This is also a continuous formulation and the Young's modulus of the joint assigned to this boundaries could be stronger or weaker than or similar to the Young's modulus of the component, depending on the kind of joint being described. The boundary-to-boundary joint modeling is expected to address the drawback of the current joint modeling because it can model joint of any complexity, as the joint follows the path of contact of the boundaries of the

component level set functions defining the joint. The boundary-to-boundary joint modeling would be explored in the future work.

CHAPTER 7

Conclusion

7.1 Dissertation summary

Thin-walled structures (TWS) are suitable for lightweight, load-bearing enclosures with various external geometries with internal reinforcements. Thin-walled structures find application in automobiles, aircrafts, ships, and industrial facilities. Past research in the field of structural design optimization have been done to make single-piece thin-walled structures less costly, lighter and of better performance. The primary drawback of these research is that complex structures are scarcely manufactured as a single piece, and this has made the optimization of single-piece structures to be of little industrial relevance.

The dissertation presented a computational method for simultaneous design and partitioning of assemblies made of thin-walled components, driven by component manufacturability. The conventional level set function for monolithic topology optimization based on a signed distance function is extended to realize a simple representation of monolithic thin-walled structures with uniform thickness, by taking advantage of the signed-distance property. A new multi-domain representation within a level set, inspired by level-set methods for multi-material topology optimization, is introduced to model multiple components, where the additional level sets specify partitioning of the level set for a monolithic thin walled structures. The geometric constraints imposed by a manufacturing process for thin-walled components, sheet metal stamping as an example, are introduced to formulate the manufacturability-driven, multi-component topology

optimization of thin-walled structures. The optimization problem is formulated as continuous optimization with respect of the level set parameters that specify overall structural geometry and its partitioning, which can be solved efficiently by gradient-based optimization algorithms. A few examples inspired by the sheet metal structures for automotive applications demonstrated the effectiveness of the new formulation to automatically design thin-walled structures made of multiple component each of which satisfies process-specific geometric constraint for component manufacturing.

7.2 Contributions

This dissertation advanced the state of the art of simultaneous designing and partitioning of thin-walled structures driven by manufacturability. Its contributions include:

1. Level-set based representation for monolithic thin-walled structures with arbitrary surface topology and geometry with a constant thickness
2. Level-set based representation for multiple subdomains (components) with arbitrary topology and geometry on the thin-walled structures in 1
3. Mathematical formulation of level-set based multi-component topology optimization of thin-wall structures based on 1 and 2, which integrates the constraints on the geometry of each subdomain imposed by component manufacturability.

While the dissertation focused on the auto-body application, it is expected that the methodology will be applicable to other domains of thin-walled structures.

7.3 Limitation and future work

While this dissertation presented the first reported work on the level-set based manufacturability-driven multi-component topology optimization tailored for thin-walled structures, several limitations are identified. These include:

- **3D implementation**: while the developed mathematical formulation is not dependent on the dimension of the design domain, only 2D implementation was demonstrated in the dissertation. This, in turn, necessitated the introduction of a fictitious substrate material with E_2 to support potentially disconnected thin strips (thin walls in 2D) of material with E_1. While this region of the substrate material could be interpreted as the projection of the thin-walls "behind" the section plane on which the design domain is defined in 2D, the current modeling does not naturally allow such interpretation since the region cannot have holes. As such, the value of E_2 is somewhat arbitrary since it is not modeling a physical material. On the other hand, 3D implementation would not need such fictitious substrate since it represents the true geometry of thin-walled structures. There is need to do more research on how to represent TWS with branching walls.
- **Joint model**: while a preliminary attempt on modeling the joint between components as the region of distinct structural property (*i.e.*, less Young's modulus than the component material) was presented in Chapter 6, it can only model straight interfaces, which is somewhat unrealistic. An improved joint model should be developed that allow arbitrary curved interfaces between components. With 3D implementation, it

would also make sense to incorporate the model of the flanges commonly adopted in the joints between thin-walled components.

- **Manufacturing constraint model**: while the cost of sheet metal stamping is proportional to both the overall size (material cost of die-set) and the perimeter length (machining cost of die-set) of the component [73], the current model only considers the overall size, as approximated by the area of MABB, but not the perimeter length. Also, the geometric constraints related to formability, such as the ones on radius-to-thickness ratio and on undercut, are not considered due to the 2D implementation.

Addressing these limitations will be the immediate future work. In a longer term, the developed formulation can be extended to other thin-wall manufacturing processes (e.g., composite manufacturing), anisotropic joint model with maximum tensile stress constraints, and multi-material structures.

References

[1] "Audi TT Body in white - Car Body Design." [Online]. Available: https://www.carbodydesign.com/gallery/2006/06/08-audi-tt-images/11/. [Accessed: 08-Jan-2020].

[2] "Candela Architecture 82892 | INFOBIT." [Online]. Available: http://www.infobit.co/candela-architecture.html. [Accessed: 08-Jan-2020].

[3] "Non IBR Steam Boiler | E-Platform India." [Online]. Available: https://www.eplatform.in/Non-IBR-Steam-Boiler-200-Kg-17-5-kg-cm2. [Accessed: 08-Jan-2020].

[4] "aircraft - Liberal Dictionary." [Online]. Available: https://www.liberaldictionary.com/aircraft/. [Accessed: 08-Jan-2020].

[5] "Electromac | Cold Stamping - Hot Stamping - Tool & Die." [Online]. Available: http://www.electromac.com/tool-die.php. [Accessed: 08-Jan-2020].

[6] "GM Is Using the Cloud to Connect Its Factory Robots | Fortune." [Online]. Available: https://fortune.com/2016/01/30/gm-cloud-factory-robots-fanuc/. [Accessed: 08-Jan-2020].

[7] S. Wang, Y. Peng, T. Wang, Q. Che, and P. Xu, "Collision performance and multi-objective robust optimization of a combined multi-cell thin-walled structure for high speed train," Thin-Walled Structures, vol. 135, pp. 341–355, Feb. 2019, doi: 10.1016/j.tws.2018.10.044.

[8] H. Ugail, "Parametric Design and Optimisation of Thin-Walled Structures for Food Packaging," Optimization and Engineering, vol. 4, no. 4, pp. 291–307, Dec. 2003, doi: 10.1023/B:OPTE.0000005389.77485.ff.

[9] Z. H. Wang, G. X. Zhang, Y. Liu, and Y. Z. Liu, "Study on the Application of Cooling Pipe in Thin-Walled Concrete Structure," Advanced Materials Research, 2011. [Online]. Available: https://www.scientific.net/AMR.163-167.1107. [Accessed: 07-Dec-2019].

[10] P. Iwicki, J. Tejchman, and J. Chróścielewski, "Dynamic FE simulations of buckling process in thin-walled cylindrical metal silos," Thin-Walled Structures, vol. 84, pp. 344–359, Nov. 2014, doi: 10.1016/j.tws.2014.07.011.

[11] T. Farsadi, M. Rahmanian, and A. Kayran, "Geometrically nonlinear aeroelastic behavior of pretwisted composite wings modeled as thin walled beams," Journal of Fluids and Structures, vol. 83, pp. 259–292, Nov. 2018, doi: 10.1016/j.jfluidstructs.2018.08.013.

[12] M.-Y. Lyu and T. G. Choi, “Research trends in polymer materials for use in lightweight vehicles,” International Journal of Precision Engineering and Manufacturing, vol. 16, no. 1, pp. 213–220, Jan. 2015, doi: 10.1007/s12541-015-0029-x.

[13] M. P. Bendsøe and N. Kikuchi, “Generating optimal topologies in structural design using a homogenization method,” Computer Methods in Applied Mechanics and Engineering, vol. 71, no. 2, pp. 197–224, Nov. 1988, doi: 10.1016/0045-7825(88)90086-2.

[14] O. Sigmund and K. Maute, “Topology optimization approaches,” Structural and Multidisciplinary Optimization, vol. 48, no. 6, pp. 1031–1055, Dec. 2013, doi: 10.1007/s00158-013-0978-6.

[15] “Metal Sintering Meets Industrial Needs with the EOS M 290 > ENGINEERING.com.” [Online]. Available: https://www.engineering.com/3DPrinting/3DPrintingArticles/ArticleID/7829/Metal-Sintering-Meets-Industrial-Needs-with-the-EOS-M-290.aspx. [Accessed: 08-Jan-2020].

[16] “Topology Optimisation Software | Materialise 3D Printing.” [Online]. Available: https://www.materialise.com/en/software/solutions-for-design/post-topology-optimization. [Accessed: 08-Jan-2020].

[17] “Hexagonal diamond lattice (Lonsdaleite); Eric Baird; January 2012; 2012-15 on eHive.” [Online]. Available: https://ehive.com/collections/4200/objects/94930/hexagonal-diamond-lattice-lonsdaleite. [Accessed: 08-Jan-2020].

[18] Y. Zhou, “Gradient-Based Multi-Component Topology Optimization for Manufacturability.” [Online]. Available: https://deepblue.lib.umich.edu/handle/2027.42/145989. [Accessed: 08-Dec-2019].

[19] S. Zargham, T. A. Ward, R. Ramli, and I. A. Badruddin, “Topology optimization: a review for structural designs under vibration problems,” Structural and Multidisciplinary Optimization, vol. 53, no. 6, pp. 1157–1177, Jun. 2016, doi: 10.1007/s00158-015-1370-5.

[20] S. Nishiwaki, M. I. Frecker, S. Min, and N. Kikuchi, “Topology optimization of compliant mechanisms using the homogenization method,” International Journal for Numerical Methods in Engineering, vol. 42, no. 3, pp. 535–559, 1998, doi: 10.1002/(SICI)1097-0207(19980615)42:3<535::AID-NME372>3.0.CO;2-J.

[21] G. Allaire, “The Homogenization Method for Topology and Shape Optimization,” in Topology Optimization in Structural Mechanics, G. I. N. Rozvany, Ed. Vienna: Springer, 1997, pp. 101–133.

[22] O. Sigmund, “A 99 line topology optimization code written in Matlab,” Structural and Multidisciplinary Optimization, vol. 21, no. 2, pp. 120–127, Apr. 2001, doi: 10.1007/s001580050176.

[23] H. Zhou, J. Zhang, Y. Zhou, and K. Saitou, “Multi-component topology optimization for die casting (MTO-D),” Structural and Multidisciplinary Optimization, vol. 60, no. 6, pp. 2265–2279, Dec. 2019, doi: 10.1007/s00158-019-02317-4.

[24] Y. Zhou and K. Saitou, “Gradient-based multi-component topology optimization for stamped sheet metal assemblies (MTO-S),” Structural and Multidisciplinary Optimization, vol. 58, no. 1, pp. 83–94, Jul. 2018, doi: 10.1007/s00158-017-1878-y.

[25] K. Liu and A. Tovar, “An efficient 3D topology optimization code written in Matlab,” Structural and Multidisciplinary Optimization, vol. 50, no. 6, pp. 1175–1196, 2014.

[26] J. A. Sethian and A. Wiegmann, “Structural Boundary Design via Level Set and Immersed Interface Methods,” Journal of Computational Physics, vol. 163, no. 2, pp. 489–528, Sep. 2000, doi: 10.1006/jcph.2000.6581.

[27] N. P. van Dijk, K. Maute, M. Langelaar, and F. van Keulen, “Level-set methods for structural topology optimization: a review,” Structural and Multidisciplinary Optimization, vol. 48, no. 3, pp. 437–472, Sep. 2013, doi: 10.1007/s00158-013-0912-y.

[28] Z. Luo, L. Tong, J. Luo, P. Wei, and M. Y. Wang, “Design of piezoelectric actuators using a multiphase level set method of piecewise constants,” Journal of Computational Physics, vol. 228, no. 7, pp. 2643–2659, Apr. 2009, doi: 10.1016/j.jcp.2008.12.019.

[29] J. Liu and Y. Ma, “A new multi-material level set topology optimization method with the length scale control capability,” Computer Methods in Applied Mechanics and Engineering, vol. 329, pp. 444–463, Feb. 2018, doi: 10.1016/j.cma.2017.10.011.

[30] H. Ghasemi, H. S. Park, and T. Rabczuk, “A multi-material level set-based topology optimization of flexoelectric composites,” Computer Methods in Applied Mechanics and Engineering, vol. 332, pp. 47–62, Apr. 2018, doi: 10.1016/j.cma.2017.12.005.

[31] M. Cui, H. Chen, and J. Zhou, “A level-set based multi-material topology optimization method using a reaction diffusion equation,” Computer-Aided Design, vol. 73, pp. 41–52, Apr. 2016, doi: 10.1016/j.cad.2015.12.002.

[32] M. Otomori, T. Yamada, K. Izui, and S. Nishiwaki, “Matlab code for a level set-based topology optimization method using a reaction diffusion equation,” Structural and Multidisciplinary Optimization, vol. 51, no. 5, pp. 1159–1172, May 2015, doi: 10.1007/s00158-014-1190-z.

[33] J. Sokolowski and A. Zochowski, “On the Topological Derivative in Shape Optimization,” SIAM Journal on Control and Optimization, vol. 37, no. 4, pp. 1251–1272, Jan. 1999, doi: 10.1137/S0363012997323230.

[34] M. Burger, B. Hackl, and W. Ring, “Incorporating topological derivatives into level set methods,” Journal of Computational Physics, vol. 194, no. 1, pp. 344–362, Feb. 2004, doi: 10.1016/j.jcp.2003.09.033.

[35] G. Allaire, F. Jouve, and A.-M. Toader, “A level-set method for shape optimization,” Comptes Rendus Mathematique, vol. 334, no. 12, pp. 1125–1130, Jan. 2002, doi: 10.1016/S1631-073X(02)02412-3.

[36] G. Allaire and F. Jouve, “A level-set method for vibration and multiple loads structural optimization,” Computer Methods in Applied Mechanics and Engineering, vol. 194, no. 30, pp. 3269–3290, Aug. 2005, doi: 10.1016/j.cma.2004.12.018.

[37] G. Allaire, F. Jouve, and A.-M. Toader, “Structural optimization using sensitivity analysis and a level-set method,” Journal of Computational Physics, vol. 194, no. 1, pp. 363–393, Feb. 2004, doi: 10.1016/j.jcp.2003.09.032.

[38] G. Allaire, C. Dapogny, G. Delgado, and G. Michailidis, “Multi-phase structural optimization via a level set method,” ESAIM: Control, Optimisation and Calculus of Variations, vol. 20, no. 2, pp. 576–611, Apr. 2014, doi: 10.1051/cocv/2013076.

[39] Y. Wang and Z. Kang, “A level set method for shape and topology optimization of coated structures,” Computer Methods in Applied Mechanics and Engineering, vol. 329, pp. 553–574, Feb. 2018, doi: 10.1016/j.cma.2017.09.017.

[40] B. Zhu, Q. Chen, R. Wang, and X. Zhang, “Structural Topology Optimization Using a Moving Morphable Component-Based Method Considering Geometrical Nonlinearity,” Journal of Mechanical Design, vol. 140, no. 8, Aug. 2018, doi: 10.1115/1.4040547.

[41] J. Bai and W. Zuo, “Hollow structural design in topology optimization via moving morphable component method,” Structural and Multidisciplinary Optimization, Aug. 2019, doi: 10.1007/s00158-019-02353-0.

[42] X. Guo, W. Zhang, and W. Zhong, “Doing Topology Optimization Explicitly and Geometrically—A New Moving Morphable Components Based Framework,” Journal of Applied Mechanics, vol. 81, no. 8, Aug. 2014, doi: 10.1115/1.4027609.

[43] W. Zhang, Y. Liu, Z. Du, Y. Zhu, and X. Guo, “A Moving Morphable Component Based Topology Optimization Approach for Rib-Stiffened Structures Considering Buckling Constraints,” Journal of Mechanical Design, vol. 140, no. 11, Nov. 2018, doi: 10.1115/1.4041052.

[44] T. Earmme, “Evolutionary Structural Optimization with Multiple Performance Constraints by Large Admissible Perturbations,” (2009).

[45] D. N. Chu, Y. M. Xie, A. Hira, and G. P. Steven, “Evolutionary structural optimization for problems with stiffness constraints,” Finite Elements in Analysis and Design, vol. 21, no. 4, pp. 239–251, Apr. 1996, doi: 10.1016/0168-874X(95)00043-S.

[46] Y. M. Xie and G. P. Steven, “Evolutionary structural optimization for dynamic problems,” Computers & Structures, vol. 58, no. 6, pp. 1067–1073, Mar. 1996, doi: 10.1016/0045-7949(95)00235-9.

[47] Y. M. Xie and G. P. Steven, “Evolutionary structural optimization for dynamic problems,” Computers & Structures, vol. 58, no. 6, pp. 1067–1073, Mar. 1996, doi: 10.1016/0045-7949(95)00235-9.

[48] X. Y. Yang, Y. M. Xie, J. S. Liu, G. T. Parks, and P. J. Clarkson, “Perimeter control in the bidirectional evolutionary optimization method,” Structural and Multidisciplinary Optimization, vol. 24, no. 6, pp. 430–440, Dec. 2002, doi: 10.1007/s00158-002-0256-5.

[49] O. M. Querin, G. P. Steven, and Y. M. Xie, “Evolutionary structural optimisation (ESO) using a bidirectional algorithm,” Engineering Computations, vol. 15, no. 8, pp. 1031–1048, Jan. 1998, doi: 10.1108/02644409810244129.

[50] X. Y. Yang, Y. M. Xie, G. P. Steven, and O. M. Querin, “Bidirectional Evolutionary Method for Stiffness Optimization,” AIAA Journal, vol. 37, no. 11, pp. 1483–1488, 1999, doi: 10.2514/2.626.

[51] X. Huang and Y. M. Xie, “A new look at ESO and BESO optimization methods,” Structural and Multidisciplinary Optimization; Heidelberg, vol. 35, no. 1, pp. 89–92, Jan. 2008, doi: http://dx.doi.org/10.1007/s00158-007-0140-4.

[52] A. R. Yildiz and K. Saitou, “Topology Synthesis of Multicomponent Structural Assemblies in Continuum Domains,” Journal of Mechanical Design, vol. 133, no. 1, Jan. 2011, doi: 10.1115/1.4003038.

[53] N. Lyu and K. Saitou, “Topology Optimization of Multicomponent Beam Structure via Decomposition-Based Assembly Synthesis,” Journal of Mechanical Design, vol. 127, no. 2, p. 170, 2005, doi: 10.1115/1.1814671.

[54] N. Lyu and K. Saitou, “Decomposition-Based Assembly Synthesis of a Three-Dimensional Body-in-White Model for Structural Stiffness,” Journal of Mechanical Design, vol. 127, no. 1, pp. 34–48, Jan. 2005, doi: 10.1115/1.1799551.

[55] F. A. Yetis and K. Saitou, “Decomposition-Based Assembly Synthesis Based on Structural Considerations,” Journal of Mechanical Design, vol. 124, no. 4, pp. 593–601, Dec. 2002, doi: 10.1115/1.1519276.

[56] C. D. Chapman, K. Saitou, and M. J. Jakiela, “Genetic Algorithms as an Approach to Configuration and Topology Design,” Journal of Mechanical Design, vol. 116, no. 4, pp. 1005–1012, Dec. 1994, doi: 10.1115/1.2919480.

[57] A. Asadpoure, J. K. Guest, and L. Valdevit, “Incorporating fabrication cost into topology optimization of discrete structures and lattices,” Structural and Multidisciplinary Optimization, vol. 51, no. 2, pp. 385–396, Feb. 2015, doi: 10.1007/s00158-014-1133-8.

[58] Y. Zhou, T. Nomura, and K. Saitou, “Multi-component topology and material orientation design of composite structures (MTO-C),” Computer Methods in Applied Mechanics and Engineering, vol. 342, pp. 438–457, Dec. 2018, doi: 10.1016/j.cma.2018.07.039.

[59] P. Jin and W. De-yu, “Topology optimization of truss structure with fundamental frequency and frequency domain dynamic response constraints,” Acta Mechanica Solida Sinica, vol. 19, no. 3, pp. 231–240, Sep. 2006, doi: 10.1007/s10338-006-0628-2.

[60] D. Guirguis, K. Hamza, M. Aly, H. Hegazi, and K. Saitou, “Multi-objective Topology Optimization of Multi-component Continuum Structures via a Kriging-interpolated Level Set Approach,” Struct. Multidiscip. Optim., vol. 51, no. 3, pp. 733–748, Mar. 2015, doi: 10.1007/s00158-014-1154-3.

[61] D. Guirguis, K. Hamza, M. Aly, H. Hegazi, and K. Saitou, “Multi-objective topology optimization of multi-component continuum structures via a Kriging-interpolated level set approach,” Structural and Multidisciplinary Optimization, vol. 51, no. 3, pp. 733–748, Mar. 2015, doi: 10.1007/s00158-014-1154-3.

[62] E. A. Kontoleontos, E. M. Papoutsis-Kiachagias, A. S. Zymaris, D. I. Papadimitriou, and K. C. Giannakoglou, “Adjoint-based constrained topology optimization for viscous flows, including heat transfer,” Engineering Optimization, vol. 45, no. 8, pp. 941–961, Aug. 2013, doi: 10.1080/0305215X.2012.717074.

[63] O. Sardan, V. Eichhorn, D. H. Petersen, S. Fatikow, O. Sigmund, and P. Bøggild, “Rapid prototyping of nanotube-based devices using topology-optimized microgrippers,” Nanotechnology, vol. 19, no. 49, p. 495503, 2008.

[64] B. Balogh and J. Lógó, “The application of drilling degree of freedom to checkerboards in structural topology optimization,” Advances in Engineering Software, vol. 107, pp. 7–12, May 2017, doi: 10.1016/j.advengsoft.2017.02.005.

[65] J. Petersson and O. Sigmund, “Slope constrained topology optimization,” International Journal for Numerical Methods in Engineering, vol. 41, no. 8, pp. 1417–1434, 1998, doi: 10.1002/(SICI)1097-0207(19980430)41:8<1417::AID-NME344>3.0.CO;2-N.

[66] O. Sigmund, “Morphology-based black and white filters for topology optimization,” Structural and Multidisciplinary Optimization, vol. 33, no. 4, pp. 401–424, Apr. 2007, doi: 10.1007/s00158-006-0087-x.

[67] A. Kawamoto, T. Matsumori, S. Yamasaki, T. Nomura, T. Kondoh, and S. Nishiwaki, “Heaviside projection based topology optimization by a PDE-filtered scalar function,” Structural and Multidisciplinary Optimization, vol. 44, no. 1, pp. 19–24, Jul. 2011, doi: 10.1007/s00158-010-0562-2.

[68] H. Li, P. Li, L. Gao, L. Zhang, and T. Wu, “A level set method for topological shape optimization of 3D structures with extrusion constraints,” Computer Methods in Applied Mechanics and Engineering, vol. 283, pp. 615–635, Jan. 2015, doi: 10.1016/j.cma.2014.10.006.

[69] M. Zhou, R. Fleury, Y.-K. Shyy, H. Thomas, and J. Brennan, “Progress in Topology Optimization with Manufacturing Constraints,” in 9th AIAA/ISSMO Symposium on

Multidisciplinary Analysis and Optimization, American Institute of Aeronautics and Astronautics.

[70] S. Zhang, A. L. Gain, and J. A. Norato, “Stress-based topology optimization with discrete geometric components,” Computer Methods in Applied Mechanics and Engineering, vol. 325, pp. 1–21, Oct. 2017, doi: 10.1016/j.cma.2017.06.025.

[71] A. M. Mirzendehdel and K. Suresh, “Support structure constrained topology optimization for additive manufacturing,” Computer-Aided Design, vol. 81, pp. 1–13, Dec. 2016, doi: 10.1016/j.cad.2016.08.006.

[72] “Following DFM Guidelines for Working with Sheet Metal,” Machine Design, 21-Sep-2016. [Online]. Available: https://www.machinedesign.com/mechanical/following-dfm-guidelines-working-sheet-metal. [Accessed: 07-Dec-2019].

[73] G. Boothroyd, P. Dewhurst, and W. A. Knight, Product design for manufacture and assembly. Boca Raton, Fl: CRC Press, 2013.

[74] M. Pohlak, R. Küttner, and J. Majak, “Modelling and optimal design of sheet metal RP&M processes,” 2005, doi: 10.1108/13552540510623620.

[75] A. Soman, S. Padhye, and M. I. Campbell, “Toward an automated approach to the design of sheet metal components,” AI EDAM, vol. 17, no. 3, pp. 187–204, Aug. 2003, doi: 10.1017/S0890060403173039.

[76] S. Li, Z. Guo, S. Cheng, and X. Zhang, “Design Optimization of Sheet Metal Stamped Parts by CAE Simulation and Back-propagation Neural Network,” Procedia Engineering, vol. 81, pp. 1023–1028, Jan. 2014, doi: 10.1016/j.proeng.2014.10.135.

[77] H. Wang, H. Xie, W. Cheng, Q. Liu, and Y. Shen, “Multi-objective optimisation on crashworthiness of front longitudinal beam (FLB) coupled with sheet metal stamping process,” Thin-Walled Structures, vol. 132, pp. 36–47, 2018.

[78] A. Wang, J. Liu, H. Gao, L.-L. Wang, and M. Masen, “Hot stamping of AA6082 tailor welded blanks: Experiments and knowledge-based cloud – finite element (KBC-FE) simulation,” Journal of Materials Processing Technology, vol. 250, pp. 228–238, Dec. 2017, doi: 10.1016/j.jmatprotec.2017.07.025.

[79] M. Merklein, M. Johannes, M. Lechner, and A. Kuppert, “A review on tailored blanks—Production, applications and evaluation,” Journal of Materials Processing Technology, vol. 214, no. 2, pp. 151–164, Feb. 2014, doi: 10.1016/j.jmatprotec.2013.08.015.

[80] G. Li, F. Xu, X. Huang, and G. Sun, “Topology Optimization of an Automotive Tailor-Welded Blank Door,” Journal of Mechanical Design, vol. 137, no. 5, May 2015, doi: 10.1115/1.4028704.

[81] S.-I. Song and G.-J. Park, “Multidisciplinary optimization of an automotive door with a tailored blank,” Proceedings of the Institution of Mechanical Engineers, Part D: Journal of

Automobile Engineering, vol. 220, no. 2, pp. 151–163, Feb. 2006, doi: 10.1243/095440706X72772.

[82] F. Xu, S. Zhang, K. Wu, and Z. Dong, “Multi-response optimization design of tailor-welded blank (TWB) thin-walled structures using Taguchi-based gray relational analysis,” Thin-Walled Structures, vol. 131, pp. 286–296, Oct. 2018, doi: 10.1016/j.tws.2018.07.007.

[83] J. Hou, J. Zhu, F. He, W. Zhang, and W. Guo, “Stiffeners layout design of thin-walled structures with constraints on multi-fastener joint loads,” Chinese Journal of Aeronautics, vol. 30, no. 4, pp. 1441–1450, Aug. 2017, doi: 10.1016/j.cja.2017.05.005.

[84] G. Hirt, C. Abratis, J. Ames, and A. Meyer, “Manufacturing of sheet metal parts from tailor rolled blanks,” Journal for Technology of Plasticity, vol. 30, Jan. 2005.

[85] G. Sun, H. Zhang, J. Fang, G. Li, and Q. Li, “Multi-objective and multi-case reliability-based design optimization for tailor rolled blank (TRB) structures,” Structural and Multidisciplinary Optimization, vol. 55, no. 5, pp. 1899–1916, May 2017, doi: 10.1007/s00158-016-1592-1.

[86] “Volkswagen MQB - Tailored rolled blanks - Car Body Design.” [Online]. Available: https://www.carbodydesign.com/gallery/2012/02/volkswagen-modular-transverse-matrix-mqb/8/. [Accessed: 08-Jan-2020].

[87] C. Wang and F. Liao, “Topography Optimization and Parametric Analysis of Bead Layout for Sheet Metal Bracket,” presented at the SAE 2010 World Congress & Exhibition, 2010, pp. 2010-01–0266, doi: 10.4271/2010-01-0266.

[88] M. M. R. Krishna, “Topology & Topography Optimization of a Drive Shaft,” presented at the 2005 SAE Commercial Vehicle Engineering Conference, 2005, pp. 2005-01–3552, doi: 10.4271/2005-01-3552.

[89] M. M. R. Krishna, “Finite Element Topography and Shape Optimization of a Jounce Bumper Bracket,” presented at the International Off-Highway & Powerplant Congress, 2002, pp. 2002-01–1468, doi: 10.4271/2002-01-1468.

[90] N. Alshabatat and K. Naghshineh, “Optimization of the Natural Frequencies of Plates Via Dimpling and Beading Techniques,” International Journal of Modelling and Simulation, vol. 32, pp. 244–254, Jan. 2012.

[91] “Tutorials > Analysis and Optimization Tutorials > Optimizing Topography.” [Online]. Available: https://solidthinking.com/help/Inspire/2018/win/en_us/optimizing_topography.htm. [Accessed: 08-Jan-2020].

[92] “Bead optimization.” [Online]. Available: https://www.3ds.com/products-services/simulia/products/tosca/structure/bead-optimization/. [Accessed: 08-Jan-2020].

[93] A. Clausen, N. Aage, and O. Sigmund, “Topology optimization of coated structures and material interface problems,” Computer Methods in Applied Mechanics and Engineering, vol. 290, pp. 524–541, Jun. 2015, doi: 10.1016/j.cma.2015.02.011.

[94] R. Dienemann, A. Schumacher, and S. Fiebig, “Topology optimization for finding shell structures manufactured by deep drawing,” Structural and Multidisciplinary Optimization, vol. 56, no. 2, pp. 473–485, 2017.

[95] R. Dienemann, A. Schumacher, and S. Fiebig, “Topology and shape optimization of sheet metals with integrated deep-drawing-simulation,” In Proceedings of 12th World Conference on Computational Mechanics, Seoul, Korea. 2016.

[96] D. E. Malen, Fundamentals of automobile body structure design. Warrendale, Pa: SAE International, 2011.

[97] N. Lyu and K. Saitou, “Decomposition-Based Assembly Synthesis of Space Frame Structures Using Joint Library,” Journal of Mechanical Design - J MECH DESIGN, vol. 128, Jan. 2006, doi: 10.1115/1.1909203.

[98] W. Zuo and K. Saitou, “Multi-material topology optimization using ordered SIMP interpolation,” Structural and Multidisciplinary Optimization, vol. 55, no. 2, pp. 477–491, Feb. 2017, doi: 10.1007/s00158-016-1513-3.

[99] M. Y. Wang and X. Wang, “‘Color’ level sets: a multi-phase method for structural topology optimization with multiple materials,” Computer Methods in Applied Mechanics and Engineering, vol. 193, no. 6, pp. 469–496, Feb. 2004, doi: 10.1016/j.cma.2003.10.008.

[100] D. Guirguis and M. F. Aly, “An evolutionary multi-objective topology optimization framework for welded structures,” in 2016 IEEE Congress on Evolutionary Computation (CEC), 2016, pp. 372–378, doi: 10.1109/CEC.2016.7743818.

[101] Z. Zhou, K. Hamza, and K. Saitou, “Decomposition Templates and Joint Morphing Operators for Genetic Algorithm Optimization of Multicomponent Structural Topology,” Journal of Mechanical Design, vol. 136, no. 2, p. 021004, Feb. 2014, doi: 10.1115/1.4026030.

[102] Y. Zhou, T. Nomura, and K. Saitou, “Multicomponent Topology Optimization for Additive Manufacturing With Build Volume and Cavity Free Constraints,” Journal of Computing and Information Science in Engineering, vol. 19, no. 2, Jun. 2019, doi: 10.1115/1.4042640.

[103] Y. Zhou, T. Nomura, and K. Saitou, “Anisotropic Multicomponent Topology Optimization for Additive Manufacturing With Build Orientation Design and Stress-Constrained Interfaces,” Volume 1: 39th Computers and Information in Engineering Conference, 2019.

[104] M. Y. Wang, X. Wang, and D. Guo, “A level set method for structural topology optimization,” Computer Methods in Applied Mechanics and Engineering, vol. 192, no. 1, pp. 227–246, Jan. 2003, doi: 10.1016/S0045-7825(02)00559-5.

[105] V. J. Challis, “A discrete level-set topology optimization code written in Matlab,” Structural and Multidisciplinary Optimization, vol. 41, no. 3, pp. 453–464, Apr. 2010, doi: 10.1007/s00158-009-0430-0.

[106] S. Osher and J. A. Sethian, “Fronts propagating with curvature-dependent speed: Algorithms based on Hamilton-Jacobi formulations,” Journal of Computational Physics, vol. 79, no. 1, pp. 12–49, Nov. 1988, doi: 10.1016/0021-9991(88)90002-2.

[107] Y. Wang, Z. Luo, Z. Kang, and N. Zhang, “A multi-material level set-based topology and shape optimization method,” Computer Methods in Applied Mechanics and Engineering, vol. 283, pp. 1570–1586, Jan. 2015, doi: 10.1016/j.cma.2014.11.002.

[108] P. Liu, Y. Luo, and Z. Kang, “Multi-material topology optimization considering interface behavior via XFEM and level set method,” Computer Methods in Applied Mechanics and Engineering, vol. 308, pp. 113–133, Aug. 2016, doi: 10.1016/j.cma.2016.05.016.

[109] S. Osher and R. P. Fedkiw, “Level Set Methods: An Overview and Some Recent Results,” Journal of Computational Physics, vol. 169, no. 2, pp. 463–502, May 2001, doi: 10.1006/jcph.2000.6636.

[110] K. Zhang, L. Zhang, H. Song, and D. Zhang, “Reinitialization-Free Level Set Evolution via Reaction Diffusion,” IEEE Transactions on Image Processing, vol. 22, no. 1, pp. 258–271, Jan. 2013, doi: 10.1109/TIP.2012.2214046.

[111] D. Guirguis, M. Aly, K. Hamza, and H. Hegazi, “Image Matching Assessment of Attainable Topology via Kriging-Interpolated Level-Sets,” in Volume 2A: 40th Design Automation Conference, Buffalo, New York, USA, 2014, p. V02AT03A002, doi: 10.1115/DETC2014-34622.

[112] K. Hamza, M. Aly, and H. Hegazi, “A Kriging-Interpolated Level-Set Approach for Structural Topology Optimization,” Journal of Mechanical Design, vol. 136, no. 1, Jan. 2014, doi: 10.1115/1.4025706.

[113] H. Sun, J. Tao, and H. Jia, “Dimension reducing of LSF parameters based on radial basis function neural network,” in INTERSPEECH, 2009.

[114] S. Townsend and H. A. Kim, “A level set topology optimization method for the buckling of shell structures,” Structural and Multidisciplinary Optimization, vol. 60, no. 5, pp. 1783–1800, Nov. 2019, doi: 10.1007/s00158-019-02374-9.

[115] S. Townsend, R. Picelli, B. Stanford, and H. A. Kim, “Structural Optimization of Platelike Aircraft Wings Under Flutter and Divergence Constraints,” AIAA Journal, vol. 56, no. 8, pp. 3307–3319, 2018, doi: 10.2514/1.J056748.

[116] X. Guo, W. S. Zhang, M. Y. Wang, and P. Wei, “Stress-related topology optimization via level set approach,” Computer Methods in Applied Mechanics and Engineering, vol. 200, no. 47, pp. 3439–3452, Nov. 2011, doi: 10.1016/j.cma.2011.08.016.

[117] K. A. James, E. Lee, and J. R. R. A. Martins, “Stress-based topology optimization using an isoparametric level set method,” Finite Elements in Analysis and Design, vol. 58, pp. 20–30, Oct. 2012, doi: 10.1016/j.finel.2012.03.012.

[118] L. Van Miegroet and P. Duysinx, “Stress concentration minimization of 2D filets using X-FEM and level set description,” Structural and Multidisciplinary Optimization, vol. 33, no. 4, pp. 425–438, Apr. 2007, doi: 10.1007/s00158-006-0091-1.

[119] G. Allaire and F. Jouve, “Minimum stress optimal design with the level set method,” Engineering Analysis with Boundary Elements, vol. 32, no. 11, pp. 909–918, Nov. 2008, doi: 10.1016/j.enganabound.2007.05.007.

[120] C. G. Lopes and A. A. Novotny, “Topology design of compliant mechanisms with stress constraints based on the topological derivative concept,” Structural and Multidisciplinary Optimization, vol. 54, no. 4, pp. 737–746, Oct. 2016, doi: 10.1007/s00158-016-1436-z.

[121] P. D. Dunning and H. A. Kim, “Introducing the sequential linear programming level-set method for topology optimization,” Structural and Multidisciplinary Optimization, vol. 51, no. 3, pp. 631–643, Mar. 2015, doi: 10.1007/s00158-014-1174-z.

[122] J. P. Blasques and M. Stolpe, “Multi-material topology optimization of laminated composite beam cross sections,” Composite Structures, vol. 94, no. 11, pp. 3278–3289, Nov. 2012, doi: 10.1016/j.compstruct.2012.05.002.

APPENDICES

APPENDIX A: Detailed derivation of the shape derivative

Interested reader are encouraged to first read Chapter 4 before reading Appendix A. Dissimilar to solid structures that have only two domains (material or void), the proposed representation of a thin-walled structure (a pair of closed offset surfaces with holes) consists of three distinct domains: material 1 defined by $(0 \leq \phi_1 \leq t) \wedge (\ \phi_2 < 0)$, shown in green, material 2 defined by$(t < \ \phi_1) \vee ((0 \leq \phi_2) \wedge (\ 0 \leq \phi_1))$, shown in yellow, and void defined by $\phi_1 < 0$, shown in white in Figure A.1. Each of these is separately taken into account in the derivation of the shape derivative.

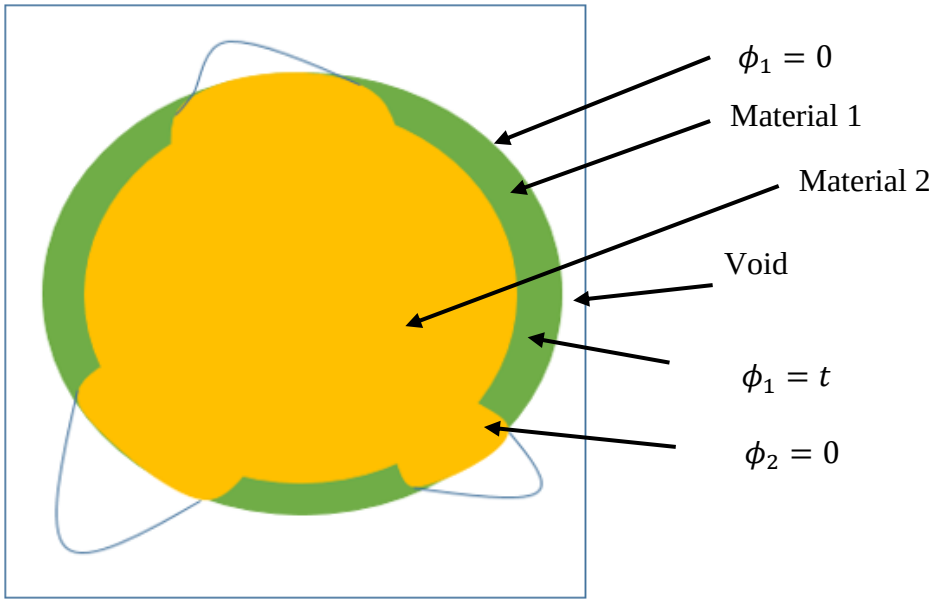

Figure A. 1 Sketch of the level set 1 and 2

The objective function is defined as:

$$J = \int_D \mathrm{e(u)}\colon \mathrm{E(\phi)}\colon e(u)\, d\Omega \qquad (10.1)$$

$$\int_D J(u)H(\phi_1,\phi_2)d\Omega = \int_D F(u)H(\phi_1,\phi_2)d\Omega + \int_\Gamma \tau u d\Gamma \qquad (10.2)$$

However, since there is no volume force,

$$\int_D F(u)H(\phi_1,\phi_2)d\Omega = 0 \quad (10.3)$$

The objective function becomes

$$\text{Min } J(u,\phi_1,\phi_2,t) = \int_{d\Omega} \tau u d\Gamma \quad (10.4)$$

$$= \int_D E_1 e(u)e(u)(H(\phi_1) - H(\phi_1 - t))(1 - H(\phi_2))\, d\Omega + \int_D E_2 e(u)e(u)(H(\phi_1) - H(\phi_1 - t))H(\phi_2)\, d\Omega + \int_D E_2 e(u)e(u)H(\phi_1 - t)\, d\Omega \qquad (10.5)$$

Subject to

$$a(u,v,\phi_1,\phi_2,t) = \int_D E_1 e(u)e(v)(H(\phi_1) - H(\phi_1 - t))(1 - H(\phi_2))\, d\Omega + \int_D E_2 e(u)e(v)(H(\phi_1) - H(\phi_1 - t))H(\phi_2)\, d\Omega + \int_D E_2 e(u)e(v)H(\phi_1 - t)\, d\Omega \qquad (10.6)$$

$$l(v) = \int_{\partial D_\tau} \tau v ds \qquad (10.7)$$

$$a(u,v,\phi_1,\phi_2,t) - l(v) = 0 \qquad (10.8)$$

$$V \le V^* \quad (10.9)$$

$$A_h \le {A_h}^* \quad (10.10)$$

$$J = \int_D E_1 e(u)e(v)(H(\phi_1) - H(\phi_1 - t))(1 - H(\phi_2))\, d\Omega + \int_D E_2 e(u)e(v)(H(\phi_1) - H(\phi_1 - t))H(\phi_2)\, d\Omega + \int_D E_2 e(u)e(v)H(\phi_1 - t)\, d\Omega \quad (10.11)$$

$$\frac{\partial J}{\partial \phi_1} = \int_D \left((E_1 - E_2)e(u)e(u) - \|Ee(u)e(u)\|_\nabla \prod_{i=1}^{N-1}(1 - k_i t) \right) H(\phi_2)\delta(\phi_1)d\Gamma - \int_D \left(E_1 e(u)e(u) - \|Ee(u)e(u)\|_\nabla \prod_{i=1}^{N-1}(1 - k_i t) \right) \delta(\phi_1)d\Gamma \quad (10.12)$$

$$\frac{\partial J}{\partial \phi_2} = \int_D (E_1 - E_2)e(u)e(u)\, H(\phi_1)\delta(\phi_2)d\Omega - \int_D (E_1 - E_2)e(u)e(u)\, H(\phi_1 - t)\delta(\phi_2)d\Omega \quad (10.13)$$

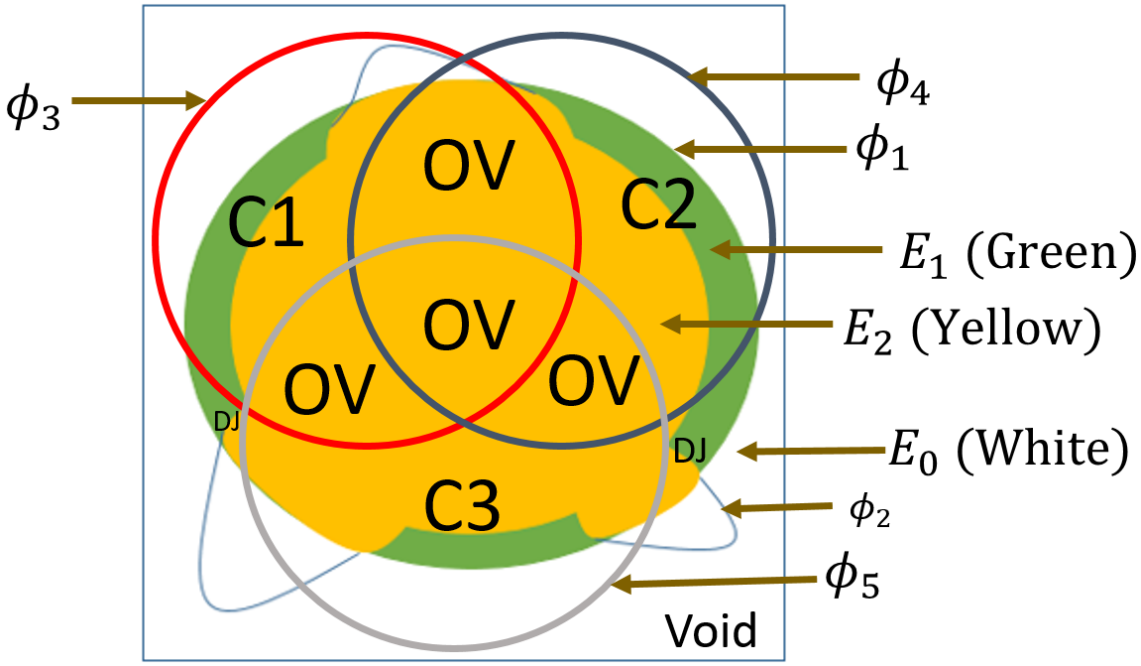

Figure A. 2 Three-component TWS partition while equality constraint is yet to be satisfied. C1 is component 1. C2 is component 2. C3 is component 3. OV is the overlap of two or more level sets. DJ is the region of ϕ_1 yet to be covered by component level set, since equality constraint is yet to be satisfied.

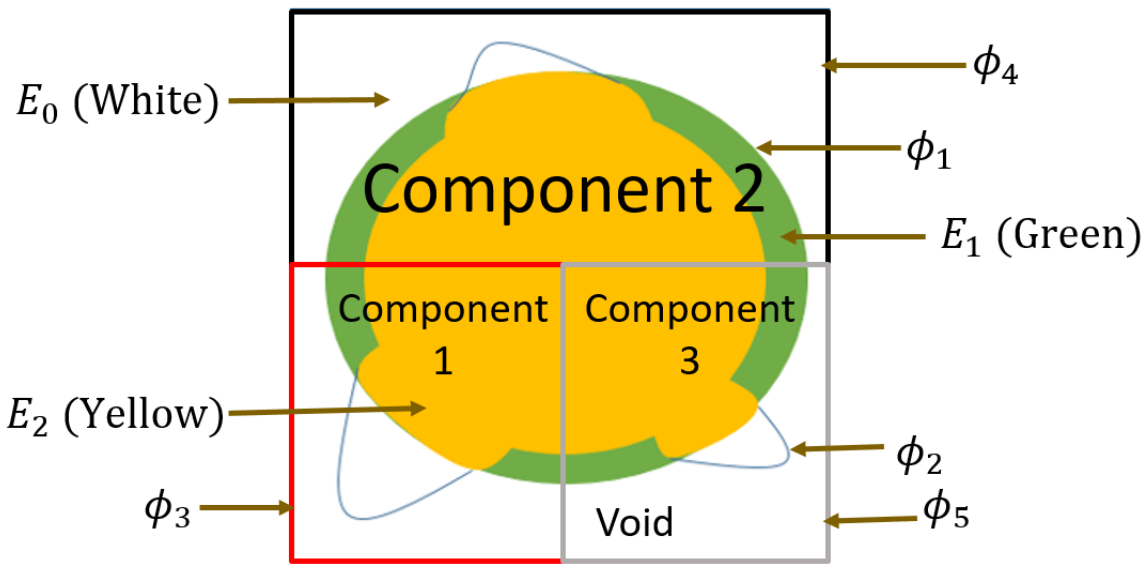

Figure A. 3 Three-component TWS partition with satisfied equality constraint

Integrating the objective function into the multi-component framework, considering three-component TWS:

$$J_{MT} = \boldsymbol{J}H(\phi_1)H(\phi_2)\left[H(\phi_3)(1-H(\phi_4)\left(1-H(\phi_5)\right) + H(\phi_4)(1-H(\phi_3)\left(1-H(\phi_5)\right) + H(\phi_5)\left(1-H(\phi_3)\right)\left(1-H(\phi_4)\right) + H(\phi_3)H(\phi_4) + H(\phi_3)H(\phi_5) + H(\phi_4)H(\phi_5) + H(\phi_3)H(\phi_4)H(\phi_5) + \left(1-H(\phi_3)H(\phi_4)H(\phi_5)\right)\right] \quad (10.14)$$

The Langragian of the objective and constraints for 3-component framework is given as:

$$L = J_{MT}(u,\phi_1,\phi_2,\phi_3,\phi_4,\phi_5,t) + \lambda^1(V-V^*) + \lambda^2(A_1-A_1{}^*) + \lambda^3(A_2-A_2{}^*) + \lambda^4(A_3-A_3{}^*) + \lambda^4(H(\phi_3)+H(\phi_4)+H(\phi_5)-1)^2 \quad (10.15)$$

The Langragian of the objective and constraints for n-component framework is given as:

$$L = J_{MT}(u,\boldsymbol{\phi},t) + \lambda^1(V-V^*) + \lambda^2(A_1-A_1{}^*) + \lambda^3(A_2-A_2{}^*) + \cdots + \lambda^{1+h}(A_h-A_h{}^*) + \lambda^{2+h}(H(\phi_3)+H(\phi_4)+\cdots+H(\phi_{2+k})-1)^2 \quad (10.16)$$

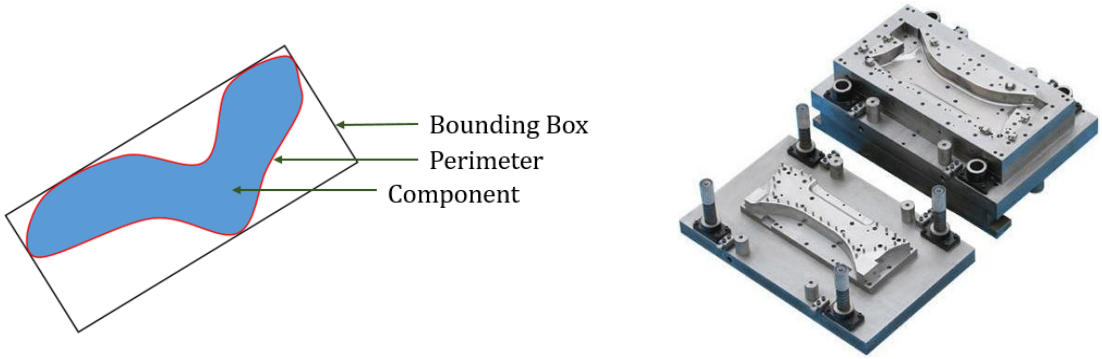

Figure A. 4 Bounding box and Perimeter of a component

Volume constraint

$$V = V_2 + \frac{rV_1}{t}\sqrt{V_2} \qquad (10.17)$$

$$V_1 = \int_D \big(H(\phi_1) - H(\phi_1 - t)\big)\big(1 - H(\phi_2)\big)d\Omega \qquad (10.18)$$

$$V_2 = \int_D \big(H(\phi_1) - H(\phi_1 - t)\big)H(\phi_2)d\Omega + \lambda_1 \int_D \big(H(\phi_1 - t)\big)\,d\Omega \qquad (10.19)$$

$$\frac{\partial V_1}{\partial \phi_1} = \int_D \left(\delta(\phi_1) - \prod_{j=1}^{N-1}(1 - \kappa_i t)\right)\big(1 - H(\phi_2)\big)d\Gamma \qquad (10.20)$$

$$\frac{\partial V_2}{\partial \phi_1} = \int_D \left(\delta(\phi_1) - \prod_{j=1}^{N-1}(1 - \kappa_i t)\right)\big(H(\phi_2)\big)d\Gamma + \int_D \left(\prod_{j=1}^{N-1}(1 - \kappa_i t)\right)d\Gamma \qquad (10.21)$$

$$\frac{\partial V_1}{\partial \phi_2} = -\int_D \big(H(\phi_1) - H(\phi_1 - t)\big)\,\delta(\phi_2)d\Gamma \qquad (10.22)$$

$$\frac{\partial V_2}{\partial \phi_2} = \int_D \big(H(\phi_1) - H(\phi_1 - t)\big)\,\delta(\phi_2) \qquad (10.23)$$

Bounding box constraint

$$\frac{\partial A_h}{\partial \phi_{\mathrm{n}}} = \frac{\partial A_h}{\partial \rho_{k_{\mathrm{n}}}} \cdot \frac{\partial \rho_{k_{\mathrm{n}}}}{\partial \phi_{\mathrm{n}}}, h\ is\ the\ component\ number \qquad (10.24)$$

$$A_h = \prod_{j_h=1}^{2} l_{j_h} \qquad (10.25)$$

$$A_h = l_{1_h} l_{2_h} \qquad (10.26)$$

$$\frac{\partial A_h}{\partial \rho_{k_{\mathrm{n}}}} = l_{1_h} \frac{\partial l_{2_h}}{\partial \rho_{k_{\mathrm{n}}}} + l_{2_h} \frac{\partial l_{1_h}}{\partial \rho_{k_{\mathrm{n}}}} \qquad (10.27)$$

$$l_{j_h} = 2\Big(\frac{1}{N}\sum_{i=1}^{N} \rho_{i_h} (z_{ji} - c_{j_h})^m\Big)^{\frac{1}{m}} \qquad (10.28)$$

$$c_{j_h} = \frac{\sum_{i=1}^{N} \rho_{i_h} z_{ji}}{\sum_{i=1}^{N} \rho_{i_h}} \qquad (10.29)$$

$$\frac{\partial c_{j_h}}{\partial \rho_{k_{\mathrm{n}}}} = \frac{\big(\sum_{i=1}^{N} \rho_{i_h} z_{ji}\big) - \big(\sum_{i=1}^{N} \rho_{i_h}\big) z_{jk}}{\big(\sum_{i=1}^{N} \rho_{i_h}\big)^2} \qquad (10.30)$$

$$\frac{\partial l_{j_f}}{\partial \rho_{k_{\mathrm{n}}}} = 2\left(\frac{1}{N}\sum_{i=1}^{N}\big(\rho_{i_h} z_{ji} - \rho_{i_h} c_{j_h}\big)^m\right)^{\frac{1-m}{m}} \frac{1}{N}\sum_{i=1}^{N}\Bigg[\big(\rho_{i_h} z_{ji} - \rho_{i_h} c_{j_h}\big)^{m-1} \cdot \left(\delta_{i_h k} z_{j_h k} - \delta_{i_h k} c_{j_h} - \rho_{i_h} \frac{\partial c_{j_h}}{\partial \rho_{k_{\mathrm{n}}}}\right)\Bigg] \qquad (10.31)$$

$$\frac{\partial l_{j_h}}{\partial \rho_{k_\mathrm{n}}} = 2\left(\frac{1}{N}\sum_{i=1}^{N}\left(\rho_{i_h} z_{ji} - \rho_{i_h} c_{j_h}\right)^{p}\right)^{\frac{1-m}{m}}$$

$$\cdot\frac{1}{N}\left\{\sum_{i=1}^{N}\left[\delta_{i_h k}(z_{j_h k} - c_{j_h})(\rho_{i_h} z_{ji} - \rho_{i_h} c_{j_h})^{m-1}\right] + \sum_{i=1}^{N} - \rho_{i_h}\frac{\partial c_{j_h}}{\partial \rho_{k_\mathrm{n}}}(\rho_{i_h} z_{ji}\right.$$

$$\left. - \rho_{i_h} c_{j_h})^{m-1}\right\} \qquad (10.32)$$

$$\frac{\partial l_{j_h}}{\partial \rho_{k_\mathrm{n}}} = 2\left(\frac{1}{N}\sum_{i=1}^{N}\left(\rho_{i_h} z_{ji} - \rho_{i_h} c_{j_h}\right)^{m}\right)^{\frac{1-m}{m}}$$

$$\cdot\frac{1}{N}\left\{\sum_{i=1}^{N}\left[\left(z_{j_h k} - c_{j_h}\right)\left(\rho_{k_h} z_{jk} - \rho_{k_h} c_{j_h}\right)^{m-1}\right]\right.$$

$$\left. + \sum_{i=1}^{N} - \rho_{i_h}\frac{\partial c_j}{\partial \rho_k}\left(\rho_{i_h} z_{ji} - \rho_{i_h} c_{j_h}\right)^{m-1}\right\} \qquad (10.33)$$

For the three-component framework,

$$L = J_{\mathrm{MT}}(u, \phi_1, \phi_2, t) + \lambda^1(V - V^*) + \lambda^2(A_1 - A_1{}^*) + \lambda^3(A_2 - A_2{}^*) + \lambda^4(A_3 - A_3{}^*) + \lambda^5(H(\phi_3) + H(\phi_4) + H(\phi_5) - 1)^2 \qquad (10.34)$$

Shape sensitivities are given by:

$$\frac{\partial L}{\partial \phi_1} = \frac{\partial J_{\mathrm{MT}}}{\partial \phi_1} + \lambda^1\frac{\partial V}{\partial \phi_1} + \lambda^2\frac{\partial A_1}{\partial \phi_1} + \lambda^3\frac{\partial A_2}{\partial \phi_1} + \lambda^4\frac{\partial A_3}{\partial \phi_1} \qquad (10.35)$$

$$\frac{\partial L}{\partial \phi_2} = \frac{\partial J_{\mathrm{MT}}}{\partial \phi_2} + \lambda^1\frac{\partial V}{\partial \phi_2} + \lambda^2\frac{\partial A_1}{\partial \phi_2} + \lambda^3\frac{\partial A_2}{\partial \phi_2} + \lambda^4\frac{\partial A_3}{\partial \phi_2} \qquad (10.36)$$

$$\frac{\partial L}{\partial \phi_3} = \frac{\partial J_{\mathrm{MT}}}{\partial \phi_3} + \lambda^2\frac{\partial A_1}{\partial \phi_3} + \lambda^3\frac{\partial A_2}{\partial \phi_3} + \lambda^4\frac{\partial A_3}{\partial \phi_3} + 2\lambda^5(H(\phi_3) + H(\phi_4) + H(\phi_5) - 1)\delta(\phi_3) \qquad (10.37)$$

$$\frac{\partial L}{\partial \phi_4} = \frac{\partial J_{\mathrm{MT}}}{\partial \phi_4} + \lambda^2\frac{\partial A_1}{\partial \phi_4} + \lambda^3\frac{\partial A_2}{\partial \phi_4} + \lambda^4\frac{\partial A_3}{\partial \phi_4} + 2\lambda^5(H(\phi_3) + H(\phi_4) + H(\phi_5) - 1)\delta(\phi_4) \qquad (10.38)$$

$$\frac{\partial L}{\partial \phi_5} = \frac{\partial J_{\mathrm{MT}}}{\partial \phi_5} + \lambda^2\frac{\partial A_1}{\partial \phi_5} + \lambda^3\frac{\partial A_2}{\partial \phi_5} + \lambda^4\frac{\partial A_3}{\partial \phi_5} + 2\lambda^5(H(\phi_3) + H(\phi_4) + H(\phi_5) - 1)\delta(\phi_5) \qquad (10.39)$$

- V_1 and V_2 are the volumes of materials 1 and 2 respectively
- E_1 and E_2 are the Young's moduli for materials 1 and 2, respectively
- r is the penalization for V_2
- λ^1, λ^2 and λ^3 are the Lagragian multipliers for the volume constraint, perimeter constraint and bounding box constraint respectively
- κ_i is the curvature of each discretized element of the level set
- H is the Heaviside function, as defined in [104]
- u is the displacement
- $e(u)$ is the strain
- N is the total number of the elements used to discretize the level set
- t is the thickness of the thin-walled structure
- δ is the derivative of the Heaviside function, as defined in [104]
- D, Ω and Γ are the fixed design domain, material domain and the boundary respectively
- m is the penalization for the p-norm
- c_j is the center of a component for the computation of dimension j
- z_j is the location of each discretized grid for the computation of dimension j

APPENDIX B: Summary of E_2 Identification from Toyota Venza Part

A-Pillar (Front Hinge Pillar)

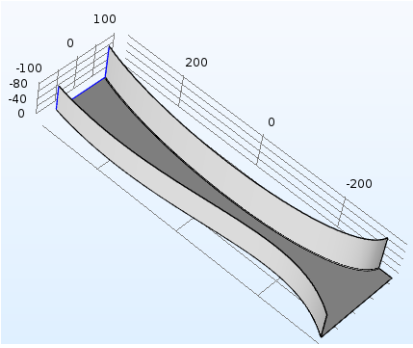

Simplified CAD version of A-Pillar

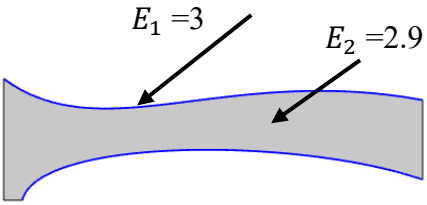

Corresponding 2D approximation that gave similar performance with similar boundary condition as 3D A-Pillar

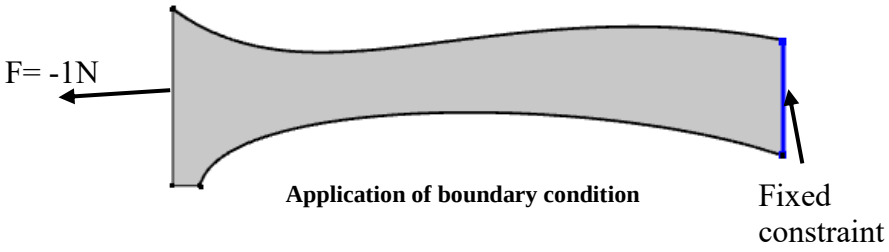

Figure B. 1 Case 1

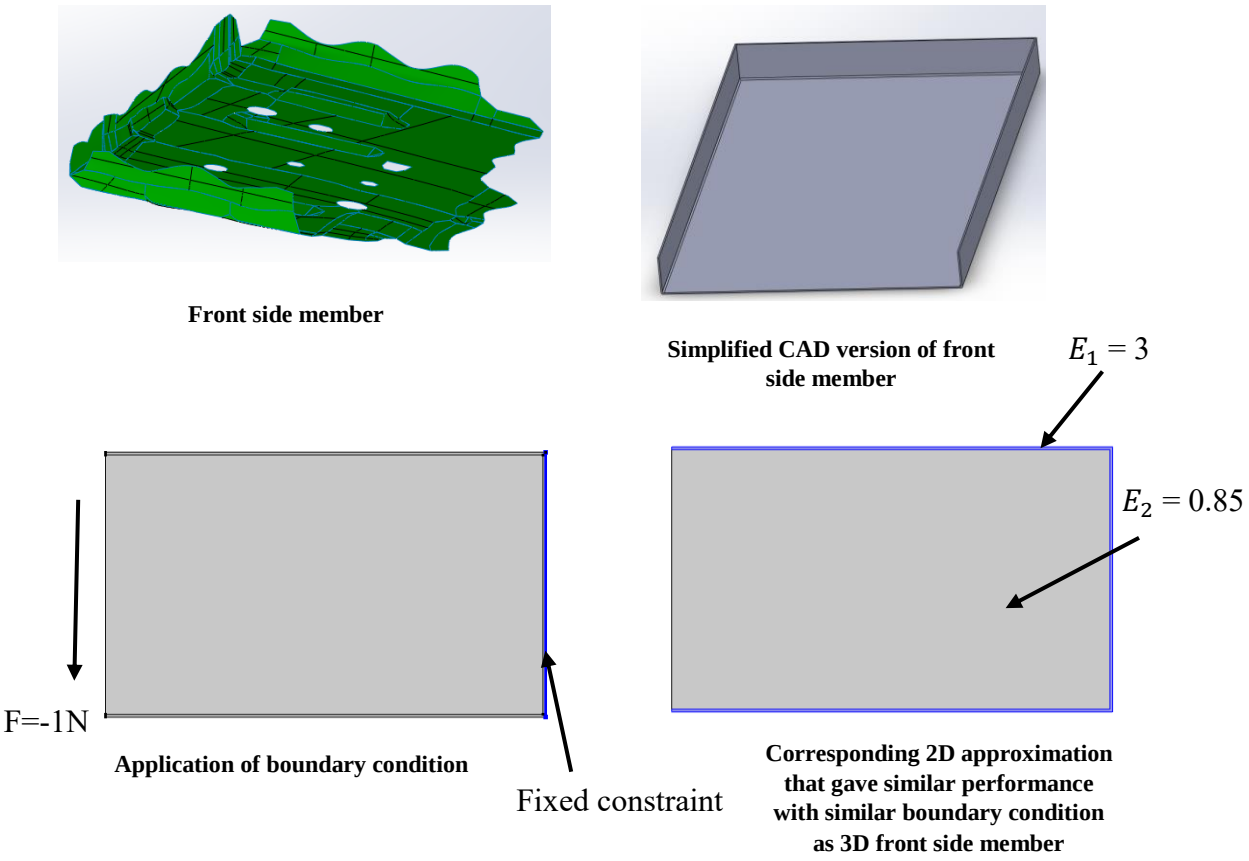

Figure B. 2 Case 2

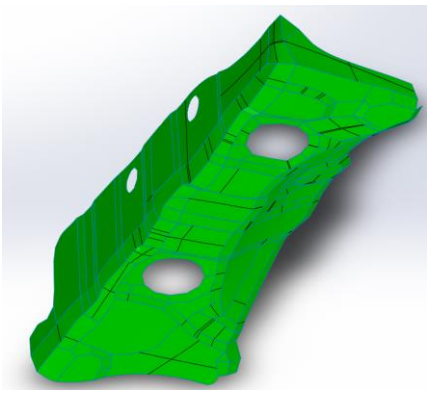

Front Apron to cowl side (Upper member inside reinforcement)

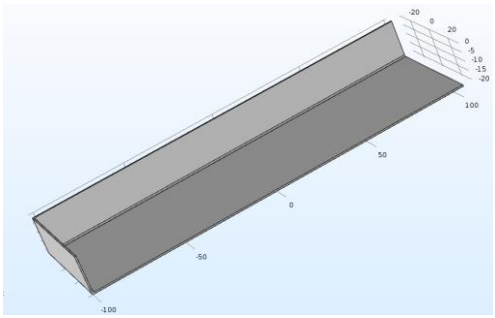

Simplified CAD version of Front Apron to cowl side

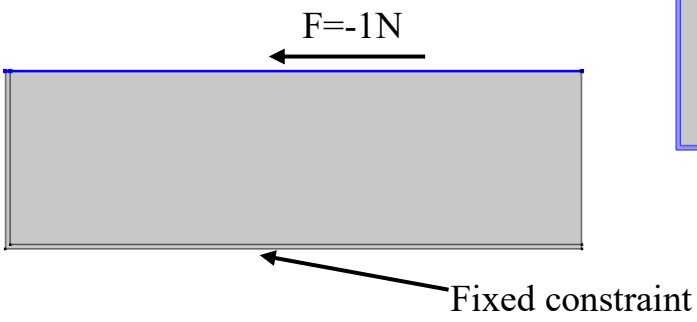

Application of boundary condition

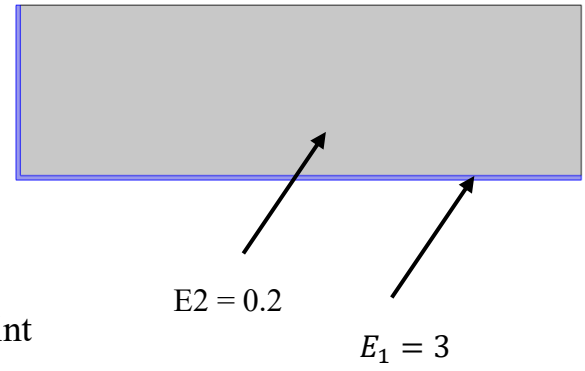

Corresponding 2D approximation that gave similar performance with similar boundary condition as 3D Front Apron to cowl side

Figure B. 3 Case 3

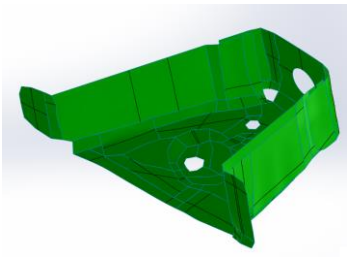

Front rail bottom

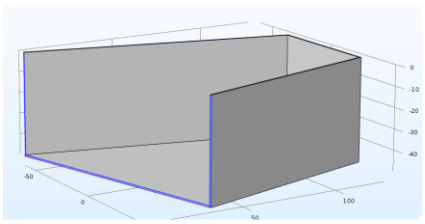

Simplified CAD version of Front rail bottom

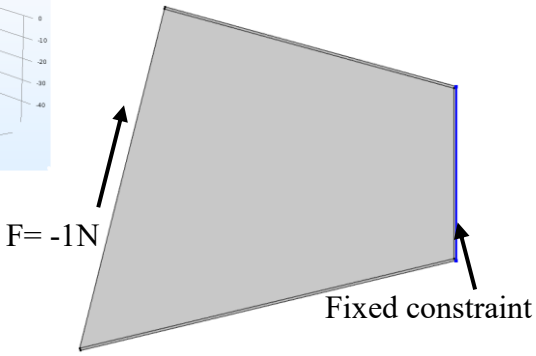

Application of boundary condition

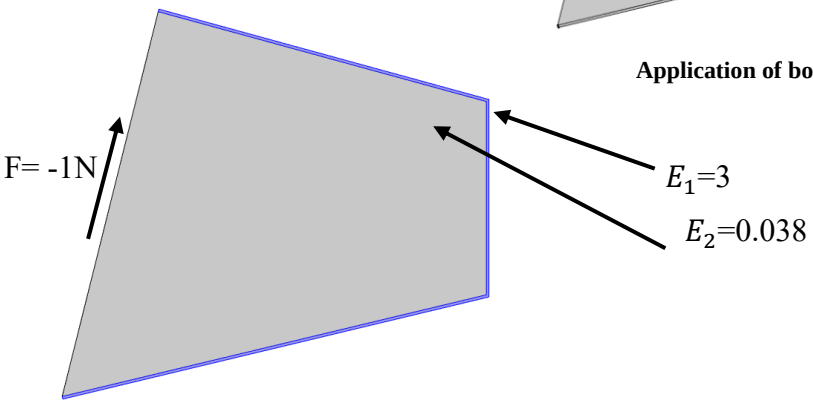

Corresponding 2D approximation that gave similar performance with similar boundary condition as 3D Front rail bottom

Figure B. 4 Case 4